CLINICAL IMPLEMENTATION OF HYPOFRACTIONATED RADIATION THERAPY FOR LUNG MALIGNANCIES

A Dissertation

by

JULIEN AVI DAN PARTOUCHE SEBBAN

Submitted to the Office of Graduate Studies of
Texas A&M University
in partial fulfillment of the requirements for the degree of

DOCTOR OF PHILOSOPHY

May 2012

Major Subject: Nuclear Engineering

Clinical Implementation of Hypofractionated Radiation Therapy for Lung Malignancies

CLINICAL IMPLEMENTATION OF HYPOFRACTIONATED RADIATION THERAPY FOR LUNG MALIGNANCIES

A Dissertation

by

JULIEN AVI DAN PARTOUCHE SEBBAN

Submitted to the Office of Graduate Studies of
Texas A&M University
in partial fulfillment of the requirements for the degree of

DOCTOR OF PHILOSOPHY

Approved by:

Chair of Committee,	John R. Ford
Committee Members,	Leslie A. Braby
	John W. Poston, Sr.
	Michael Walker
Head of Department,	Yassin A. Hassan

May 2012

Major Subject: Nuclear Engineering

ABSTRACT

Clinical Implementation of Hypofractionated Radiation Therapy

for Lung Malignancies. (May 2012)

Julien Avi Dan Partouche Sebban, M.E. Fondation EPF, M.S. Texas A&M University

Chair of Advisory Committee: Dr. John R. Ford

For patients with oligometastases, metastases limited in number and site, the use of radiation therapy treatment with a hypofractionated dose scheme has been proposed as a potential ablative approach. There are a limited number of prospective studies looking at hypofractionated radiation therapy (HRT) for lung oligometastasis. Normal lung tissue complication and radiation planning technique are significant limiting factors for the implementation of hypofractionated lung metastasis. The problem statement of this study is how to improve the clinical implementation of HRT for lung metastasis exploring lung toxicity predictors, and developing an efficient radiation planning method.

In the first study, we analyzed the dose distribution for 28 patients with lung oligometastasis and treated with HRT to multiple metastases in the lungs. We identified several significant predictors for lung radiation pneumonitis (RP) including the mean lung dose (MLD), V13 and V20. In addition a dose-effect relation between the lung normalized total dose (NTD) and RP may exist up to 48 Gy in three fractions. The dose-response parameters derived in our study appear to agree with other hypofractionated results published in the literature.

In the second study, we used an inverse planning algorithm to develop a new radiation planning method by limiting the number of segments per beam angle down to 1 segment. Single segment plans were able to significantly improve tumor coverage and conformality, reduce the

risk of lung RP, while simplifying the planning process and delivery. Target conformality and normal lung tissue sparing did not gain much improvement from an increase of plan complexity to five segments over the simplified one segment technique. The automation of our method is a good alternative to more traditional methods and offers significant dosimetric benefits.

In the third study, we verified the single segment planning technique via patient specific quality assurance (QA) in a motion phantom. We found good agreement between calculated and measured doses via thermoluminescent detectors (TLD) inside the target. A dose to distance agreement of 3%/3 mm and 2%/2 mm between calculation and film measurements for representative plans in a motion phantom was verified at 98.99% and 97.15%, respectively.

DEDICATION

To my parents, my brother and my sister

ACKNOWLEDGEMENTS

I would like to thank my committee chair, Dr. Ford, and my committee members, Dr. Braby, Dr. Poston, and Dr. Walker, for their assistance and supervision throughout the course of this research.

I also would like to thank all the members of the radiation oncology department at University of Chicago for their guidance and help throughout the course of this research.

Finally, thanks to my mother and father for their encouragement and to my brother and sister for their support.

TABLE OF CONTENTS

Page

ABSTRACT iii

DEDICATION v

ACKNOWLEDGEMENTS vi

TABLE OF CONTENTS vii

LIST OF FIGURES ix

LIST OF TABLES xi

1. INTRODUCTION 1

    1.1 Stereotactic radiation therapy 1
    1.2 Radiation dose fractionation and cellular response model 2
    1.3 Radiation therapy in the management of lung malignancies 5
    1.4 The challenges of hypofractionated radiation therapy..... 7
        1.4.1 Toxicities at high dose per fraction..... 7
        1.4.2 Radiation therapy planning techniques in the context of HRT 9
        1.4.3 Investigation on a newly developed planning technique..... 12
        1.4.4 Hypofractionated image guided radiation therapy (HIGRT)..... 15
        1.4.5 Quality assurance (QA)..... 21
    1.5 A proposal to improve the implementation of HRT 21

2. AIM 1: DETERMINE THE RELATION BETWEEN THE INCIDENCE OF NORMAL LUNG TOXICITY AND THE DOSE DISTRIBUTION FOR HYPOFRACTIONATED LUNG PATIENTS 23

    2.1 Materials and methods..... 23
        2.1.1 Study object..... 23
        2.1.2 Toxicity and dosimetric analysis..... 25
    2.2 Results 27
    2.3 Discussion 33
    2.4 Conclusion 36

3. AIM 2: DEVELOP A NOVEL RADIATION PLANNING METHOD FOR LUNG PATIENTS TREATED WITH HRT 37

    3.1 Materials and methods..... 37
        3.1.1 Study object..... 37
        3.1.2 Study design..... 39
        3.1.3 Treatment plan evaluation..... 40

3.1.4 Statistics 41
3.2 Results 41
3.3 Discussion 56
3.4 Conclusion 59

4. AIM 3: VERIFY AND VALIDATE THE PLANNING TECHNIQUE PRESENTED IN AIM 2 VIA DOSIMETRIC QA DELIVERED ON A MOTION PHANTOM 60

4.1 Materials and methods…….. 60
4.2 Results 64
4.3 Discussion 70
4.4 Conclusion 72

5. CONCLUSION AND FUTURE WORK 73

REFERENCES 75

VITA 94

LIST OF FIGURES

FIGURE		Page
1	Single Dose vs. Multiple Dose fractionation (a); Normal Tissues vs. Tumor Tissues during multiple-fraction exposure (b), for typical normal tissue with low α/β (~ 3 Gy) and tumor cell with high α/β (~ 10 Gy).	4
2	Diagram illustrating the therapeutic ratio in radiation therapy	9
3	Dose profiles across the target between conventional (—) and hypofractionated dose fractionation plans (- -).	11
4	Axial, coronal and sagital views of a patient treated with HRT to a lesion in the lung delineated in green. 3D/3D registration of the planning CT data set (left) and the CBCT (right) acquired before treatment shows adequate and optimum patient and tumor localization and positioning	19
5	(a) Diagram of coordinate systems used in conventional radiotherapy (left) and stereotactic body radiotherapy (right). (b) Example of an Elekta body frame	20
6	Smithers alpha cradle (Smithers Medical Products, North Canton, USA) immobilization device	20
7	NTD plotted as a function of MLD with linear regression modeling their relationship	30
8	Observed incidences of RP Grade ≥ 2. Error bars shows the 68% confidence interval (CI)	31
9	Maximum likelihood estimation of NTCP plotted as a function of NTD (-), and 68% confidence interval of NTCP plotted as a function of NTD (- -)……..	32
10	Bar graphs distribution of CI (top) and R100 (bottom)	43
11	HI distribution depending on PTV volumes	45
12	Percentage difference for R100 and CI, for 1 segment and 5 segments plans and relative to 3DCRT plans	47
13	Spinal cord, esophagus and heart maximum point dose for each patient	49
14	Normal lung tissue complication probability for each patient and each of the three planning techniques, 3DCRT, 1 segment and 5 segments plans.	52

15 DVHs for PTVs receiving 30 and 36 Gy and for the whole lung minus GTV for Case #1. 54

16 Isodose curves for Case #1, showing 3DCRT (top), 1 segment (middle) and 5 segments (bottom) plans for all four lesions 55

17 QUASAR respiratory motion used for patient-specific QA..... 61

18 Lung insert with tissue equivalent target used to simulate a target in lungs in the respiratory phantom..... 61

19 Tissue equivalent target used to simulate a tumor is lung with TLD positions 62

20 Geometric representation of dose distribution evaluation criteria using the combined dose difference and dose to agreement criteria defined by Low *et al.* [134]..... 63

21 Axial view of the phantom with treatment beams applied from patient #11 (top), 3D view of the phantom with treatment beams (bottom)..... 65

22 Optimized MLC apertures for patient #11 66

23 (Left) Isodose curves for LUL target treated for patient #11 with nine beams (25%, in blue, 50% in pink, 80% in orange, 100% in red, and 105% in blue isodose regions are displayed. (Right) The nine beams were applied and computed to the respiratory phantom geometry, and the same isodose regions are displayed.. 67

24 (left) Dose fluence inside the target computed with the planning system. Images of the scanned Radiochromic films after being exposed with the treatment beams copied from patient #1 68

25 Dose profiles along the y direction (cranial-caudal), showing the planned dose profile in blue, the measured dose profile in red, and the difference between both profiles in green. 68

26 Histogram of the measured counts sorted by their gamma value. 99.84% of all the counts passed the criteria of 3%/3mm with a gamma values smaller than 1.. 69

LIST OF TABLES

TABLE		Page
I	Summary of reviewed dose constraints in the context of standard fractionation[39] and in the context of HRT[40]. (Based on a whole lung volume of 3000 cc, and maximum dose constraints are given for point dose of at least 0.035 cc)	8
II	Description of dose cohorts in the study	24
III	Metastases locations sorted by their number of treated lesions; RLL: right lower lobe, RUL: right upper lobe, RML: right medial lobe, LUL: left upper lobe, LLL: left lower lobe, LML: left medial lobe.	24
IV	Summary of patients showing Grade ≥ 2 and Grade ≤ 1 toxicity	28
V	Summary of the p values for the lungs and PTV metrics.....	29
VI	Origin of oligometastases for the two subgroups of patient experiencing RP Grade ≥ 2 and RP Grade ≤ 1	29
VII	Study object: multiple oligometastases' cohort.....	38
VIII	RTOG dose limits for hypofractionated lung radiation therapy.....	41
IX	Summary of PTV metrics and differences between 1-segment, 5-segments and 3DCRT plans.	42
X	Percentage difference of the 1- and 5-segments plans relative to the 3DCRT plans for R100 and CI	46
XI	Summary of maximum point dose for the spinal cord, esophagus and heart for all of the three planning techniques, 3DCRT, 1-segment and 5-segments plans.	48
XII	Summary of lung metrics (top), p values comparison for all the lung metrics between each of the three planning techniques, 3DCRT, 1-segment and 5-segments plans.....	51
XIII	Dose at seven locations inside the target measured with TLD for patient #1, 10 and 11. All doses are expressed in percentage relative to the planned.	67
XIV	Summary of the passing rates for patients #1, 10 and 11, with both criteria, 3%/3mm as well as 2%/2mm.....	70

1. INTRODUCTION

1.1 Stereotactic radiation therapy

Since the early 1990s, stereotactic body radiation therapy (SBRT) delivering high radiation doses to extracranial targets has emerged based on the long-term experience of stereotactic radiosurgery (SRS). SRS is the delivery of a large radiation dose to intracranial targets using a dedicated stereotactic localization system. It was first described in 1951 by Lars Leksell[1], a neurosurgeon at the Karolinska Insitute in Sweden, to treat lesions in the brain with a single, very-high dose of radiation. Leksell first developed an instrument with a stereotactic coordinate system to guide the surgical instrument to a specific point and reduce entry damage during biopsies. He applied the same stereotactic coordinate system to better localize and treat intracranial lesions during radiation therapy. The goal of SRS was to replace surgical procedures. The earliest category of patients treated with SBRT was patients with medical conditions for which no other treatment options were available; targeting lesions in the spinal cord[2], the lungs and liver[3-5]. Early results were encouraging with good tumor response and low toxicities. At the beginning it was unclear which dose regimen was the most efficient but investigators at the Karolinska Insitute established a three-fractions regimen based on accumulated experience. Other experiences in the late 1990s and early 2000s in Japan[3] and the US[4-7], investigated of the feasibility of safe and efficient stereotactic radiation therapy for extracranial targets with promising outcomes.

This dissertation follows the style of *Medical Physics*.

1.2 Radiation dose fractionation and cellular response model

Soon after Wilhelm Roentgen discovered x-rays in 1895, radiation therapy (RT) was used to treat tumors. RT was delivered in single fractions with often good tumor response but also many incidences of intolerable toxicities. The techniques for radiation delivery used at that time were not advanced, often resulting in exposure of large volume of normal tissue and excessive skin toxicities due to low-energy x-rays. An alternative way of delivering RT was to deliver small fractions of radiation protracted over a period of time. In the 1900s to 1930s a series of experiments performed in France demonstrated the biological basis for fractionated radiation therapy. In a classic radiobiology experiment, Bergonie and Tribondeau showed that rams could be sterilized by exposing testes to a single dose of radiation also inducing extensive skin damage, while if the radiation was fractionated over a period of weeks with daily irradiation, sterilization was possible without producing skin damage. From these experiments it was postulated that fractionated radiation therapy can produce better tumour control, without inducing toxicities, than a single large dose of radiation.

The response of mammalian cells to fractionated photon irradiation can be described by the four "R's" of radiotherapy: repair, repopulation, reoxygenation, and redistribution[8], also referred to as the five "R's" with the addition of radiosensitivity[9], which accounts for intrinsic cell sensitivity to radiation. Repair involves complex pathways of sublethal damage repair with variety of enzymes and proteins[10], repopulation involves cells dividing while receiving radiation doses, redistribution involves a rearrangement of proliferating cells' cycle phases, and reoxygenation involves an oxygen "reload" of hypoxic cells during the course of irradiation making them more radiosensitive.

Via reoxygenation and redistribution, tumor cells that were hypoxic cells or in a less radiosensitive phase can be targeted better by fractionated radiation therapy thereby increasing

tumor damage. In addition, fractionated radiation therapy enhances sublethal damage repair in late reacting tissue and repopulation in early reacting tissue, both improving normal tissue sparing. However tumor cells can also repair and repopulate, and normal tissue cells can become more radiosensitive during redistribution and reoxygenation. Overall the main benefit of fractionated radiation therapy is to spare normal tissue from any complication. Regarding tumor cell kill, fractionation is therefore more of a compromise than a real advantage, and the acceptance of small fraction size dose regimen was predominantly established based on empirical and practical observation rather than randomized trials.

The response to fractionated irradiation of mammalian cells is noticeable in cell survival curves, representing the cell surviving fraction on a logarithmic scale against the dose on linear scale. The response of normal and tumor tissues depends on the temporal pattern of radiation delivery (e.g., dose rate and dose fractionation). The linear quadratic (LQ) model for cell survival is the most commonly used model to describe cell survival. The LQ formalism is attractive because it has minimum number of adjustable parameters needed while explaining trends in cell survival as a function of dose and dose rate with acceptable accuracy. The LQ formalism[11,12] expresses the surviving fraction in terms of a damage coefficient α for lethal lesions produced in the cell deoxyribonucleic acid (DNA) by one-track action, and a damage formation coefficient β for lethal lesions produced in the cell DNA by two-track action, representing respectively a linear and quadratic component. The dose at which these two components are equal is represented by the α/β ratio. The LQ model is widely used in clinical applications and has been discussed extensively in the literature [13,14]. It is implemented as follows, where SF is the surviving fraction, and d is the radiation dose:

$$SF = e^{-\alpha d - \beta d^2}. \quad (1)$$

Survival curves typically show an initial slope, followed by a shoulder region, and a nearly straight line at higher doses[15]. In general late reacting tissues exhibit a greater shoulder with lower α/β ratio of about 3 Gy, while tumor cells or early reacting tissues show a smaller shoulder with greater α/β ratio of about 10 Gy. Therefore the LQ model suggests that when the α/β ratio of tumors cells is greater than the one of the normal tissue cells, then a lower dose per fraction will be more effective[16]. On the contrary when α/β ratios for normal tissue and tumor cells are about the same a larger dose per fraction will be more effective, as it has been suggested for prostate cancer[17]. An idealized fractionation experiment survival curve is shown in Fig. 1 illustrating the influence of the shoulder for single and multiple fractions regimen.

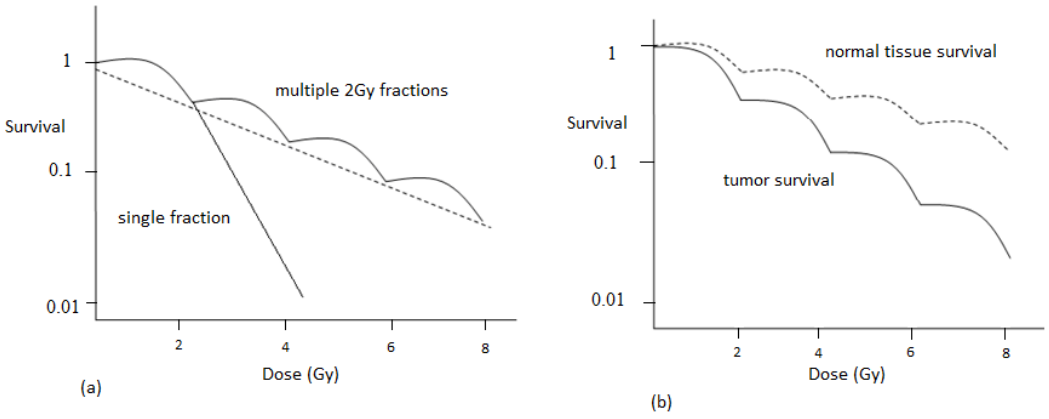

Fig. 1. Single Dose vs. Multiple Dose fractionation (a); Normal Tissues vs. Tumor Tissues during multiple-fraction exposure (b), for typical normal tissue with low α⁄β (~ 3 Gy) and tumor cell with high α⁄β (~ 10 Gy).

The LQ model has also been used to predict the therapeutic advantages of hypofractionated radiotherapy. The biological effective dose (BED) is derived from the LQ

equation; it is defined as the total dose delivered in an infinitesimal small dose per fraction and giving the same biological effect as a fractionation delivering a total dose D with d being the dose per fraction:

$$\mathrm{BED} = \mathrm{D}\left(1 + \frac{\mathrm{d}}{\alpha/\beta}\right), \quad (2)$$

The BED equation can be used to compare different dose fractionation schemes. The NTD[18] is the total dose, delivered in reference fractional doses of d_0, and having the same biological effect as a total dose D delivered in n fractions. The NTD formula is obtained by equating the BED of the fractionation schemes and is defined as follows:

$$\mathrm{NTD}\left(\mathrm{d}_0\right) = D\frac{\left(\alpha/\beta + D/n\right)}{\left(\alpha/\beta + d_0\right)}. \quad (3)$$

The NTD evaluation can be particularly useful in order to evaluate the dose necessary to achieve a desired tumor control. For example, for a non-small-cell lung cancer (NSCLC) Martel *et al*.[19] suggested that a minimum dose of 84 Gy (in 2 Gy fractions) may be necessary to achieve significant probability of tumor control. Consequently from equation 3, assuming an α/β ratio of 10 Gy, 60 Gy delivered in 3 fractions is equivalent to an NTD of 150 Gy in 2 fractions and would be much more biologically potent than 60 Gy delivered in 2 Gy fractions. Larger fractional doses with reduced cell repopulation due to fewer fractions and shortened therapy course can result in greater lethal cell damage.

1.3 Radiation therapy in the management of lung malignancies

According to Langley and Fidler[20] most deaths from solid cancers are caused by metastases that are resistant to conventional therapies. In a seminal study published in 1889,

Stephen Paget[21] observed that the distribution of metastases among 735 cases of breasts cancer was not random, he postulated that some type of tumor cells grow preferably in some particular organs, a theory commonly referred to as the "seed and soil" hypothesis. For example, lung is the second most common site for metastasis, because of its dense vascular area, the lung parenchyma presents a fertile microenvironment for the growth of secondary tumors. Primary cancers of the breast, colon, kidney, bladder, head and neck, and skin melanoma show higher probability of spreading to the lungs[22]. Unlike patients with locally confined disease who are usually treated with curative intent, patients with distant metastases are usually treated with palliative intent using systemic chemotherapy along with targeted local radiation therapy for the relief of symptoms.

In the spectrum of cancer growth, Hellman and Weichelsbaum[23] suggested the existence of an oligometastatic stage, between locally confined and widely metastatic, when spread of tumor cells is limited in quantity and location. They implied that a localized treatment of the metastases with curative intent is feasible. Complete resection of clinically detectable metastatic tumors together with systematic chemotherapy is believed to be a curative approach[24] in the management of lung metastases. In addition, the International Registry of Lung Metastases[25] reported a 5-year survival of 36% for patients with complete resection of lung metastases, compared with 13% for patients without resection. Therefore, it has been demonstrated that surgical resection of lung metastases may increase survival with possible curative intent.

For primary lung tumors, radiation therapy with a high dose per fraction has been shown to achieve local control comparable with surgical resection. A Phase II study looked at 70 unresectable Stage I and II Non-small cell lung cancer (NSCLC) patients treated in 3 fractions to a total dose of 60-66 Gy[26]. With a median follow-up of 50.2 months, the rate of local control, defined as the cessation of cancer growth at the site of origin, at 3 years was 88.1%. Other recent

clinical trials have shown encouraging outcomes and high control rates for patients with early-stage, non-resectable NSCLC[4, 27-30] treated with a hypofractionated dose regimen.

Similarly the ablative nature of HRT as a substitute for surgical resection, can be of great interest when targeting oligometastasis in lungs. Used as a noninvasive procedure to ablate metastatic tumors in lung, investigators have achieved satisfactory local controls using HRT[31-33]. Clinical trials have reported encouraging outcomes with high local control rates: Blomgren *et al.*[34] delivered 21-66 Gy in 1-3 fractions to 13 patients with a total of 17 lesions, and achieved an estimated local control of 83%; Nagata *et al.*[35] delivered 48 Gy in 4 fractions to 9 patients with a total of 9 lesions, and achieved an estimated local control of 67%; Onimura *et al.*[36] delivered 48-60 Gy in 8 fractions to 20 patients with a total of 32 lesions, and achieved an estimated local control of 69%; Wulf *et al.*[37] delivered 30-42 Gy in 3 fractions to 20 patients with a total of 32 lesions, and achieved an estimated local control of 71%; Rusthoven *et al.*[38] delivered 60 Gy in 3 fractions to 38 patients with a total of 63 lesions, and achieved a 96% local control.

Successful outcomes of early clinical trials have proved the efficacy of HRT for the management of metastatic lung tumors; however, the enhanced cell killing and reduced cell repair inevitably pose greater risks of severe normal tissue damages and irrecoverable loss of function of healthy organs. HRT presents radiobiological challenges as well as physics challenges addressed in the next section.

1.4 The challenges of hypofractionated radiation therapy

1.4.1 Toxicities at high dose per fraction

Organs-at-risk (OAR) dose tolerances for HRT are established to be much lower than those for the conventional dose schemes (1.8 Gy-2.0 Gy per fraction). Table 1 presents examples

of dose constraints for selected organs given in the context of standard dose fractionation, based on the QUANTEC review[39], as well as "suggested" dose constraints in the context of HRT found in the literature[40].

Phase I and II clinical trials showed that treatments were generally safe if normal tissue doses were less than the suggested tolerance levels. However, cases with severe toxicity have been reported; most common toxicities include chest pain, esophagitis, and rib fractures, spinal cord disease (myelopathy) and RP[41]. Particularly, RP occurred at much lower dose levels, and is considered the major limiting factor of applying HRT in the management of lung malignancies.

Table. I. Summary of reviewed dose constraints in the context of standard fractionation[39], and in the context of HRT[40]. (Based on a whole lung volume of 3000 cm^3, and maximum dose constraints are given for point dose of at least 0.035 cm^3)

Dose constraints			
Tissue	Endpoint	Standard dose regimen (1.8-2.0Gy per fraction)	Hypofractionated dose regimen (Delivered in 3 fractions)
Spinal cord	Myelopathy	Max dose≤50Gy	Max dose≤18Gy
Esophagus	Esophagitis	Mean dose≤34Gy	V17.7Gy≤5cc
Heart	Pericarditis	Mean dose≤26Gy	V24Gy≤15cc
Whole lung	Pneumonitis	V20Gy≤30%	V12.4Gy≤30%*

One of the most difficult tasks is to design and evaluate a treatment plan that obtains an optimal therapeutic ratio for a patient. Figure 2 shows the shift in therapeutic ratio, defined as the

separation between the probability of tumor control and the probability of normal tissue complication. An optimum radiation plan increases the therapeutic ratio by increasing the likelihood of tumor control and decreasing the likelihood of normal tissue complication.

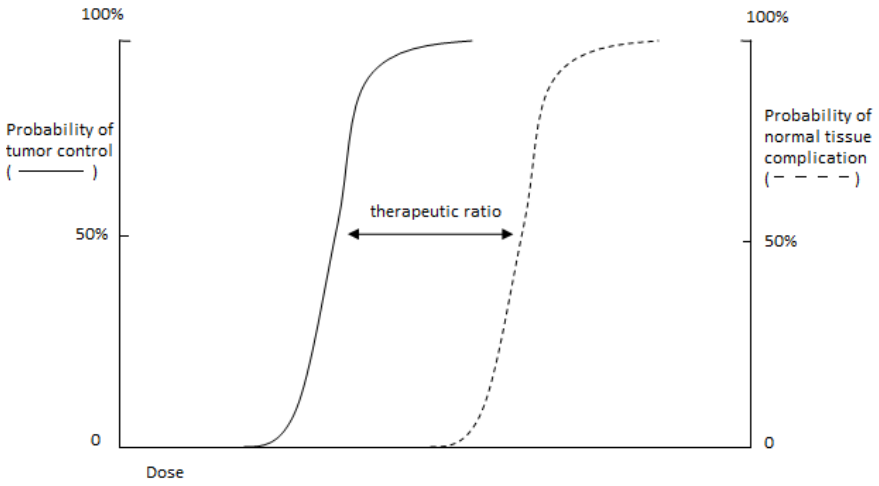

Fig. 2. Diagram illustrating the therapeutic ratio in radiation therapy

The full potential of dose hypofractionation in improving the therapeutic ratio will be reached only when the clinicians will be able to use quantitative tools to guide the optimization of a treatment plan.

1.4.2 Radiation therapy planning techniques in the context of HRT

A planning technique must suit the goal of dosimetric endpoints. In principle most commercially available treatment units producing high-energy photons (4-10 MV) are acceptable

for hypofractionated radiation therapy. Among the various machines used we can distinguish between the conventional linear accelerators (linac) using dedicated image guidance tools such as Novalis, Trilogy or TrueBeam (Varian Medical Systems, Palo Alto, USA), Synergy (Elekta, Stockholm, Sweden) or Artiste (Siemens, Munich, Germany), and the specialized dose painting accelerators such as Tomotherapy (Accuray, Sunnyvale, USA) or Cyberknife (Accuray, Sunnyvale, USA). In the context of lung HRT studies investigating the use of Cyberknife[42-43], and Tomotherapy[44-46], Ding *et al.*[47] presented a comparison between linac-based and Cyberknife therapy. They concluded that both techniques provide adequate target dose coverage and that target location may be a good indicator for the most appropriate technique. Mavroidis *et al.*[48] presented a comparison between linac-based therapy and Tomotherapy for lung HRT with small dosimetric differences between the two techniques. Among the linac-based techniques, we can also distinguish the static conformal beams, the Intensity Modulated Radiation therapy (IMRT)[49], and arc techniques[50-52]. There is no consensus which technique is best suited for lung hypofractionated radiation therapy, and in this study we are going to focus on linac-based techniques.

When treating a lung tumor, the most simple and straightforward beam arrangements are two beam angles anterior-posterior (AP/PA) to 40 Gy followed by opposed obliques to 60 Gy. In this way, a certain volume of normal lung would be exposed to high doses in order to minimize the volume of normal lung exposed to low doses, so that the MLD and the amount of normal lung exposed to radiation will be minimal, and the maximum dose to the spinal cord will be below tolerance (45-50 Gy). In conventional 3DCRT, the planner manually adjusts the gantry angles, collimator angles, the couch angles, the beam apertures, and the beam weightings many times during the evolutional process of dose distribution optimization. Early experience in HRT demonstrated that dose to the normal lung tissues immediately surrounding the tumors can be

very likely correlated to the incidence of RP, and this end-point requires multiple non-coplanar, non-opposing beams to make the dose distribution highly conformal to the target. The low-dose region is spread over a larger volume of normal lung to improve high dose conformality to the planning target. A sharp dose gradient is achieved by using small fields, with often no or negative block to target margin; thus resulting in a rapid dose fall-off and inhomogeneous dose distribution inside the target with high doses at the center. Similar to SRS planning the dose is prescribed to the 80-90% isodose line. Having very high doses at the center of the target is particularly of interest since some tumors often present radioresistant hypoxic cells at their center[53]. Figure 3 shows the difference in dose profiles across the target between conventional and hypofractionated dose fractionation plans.

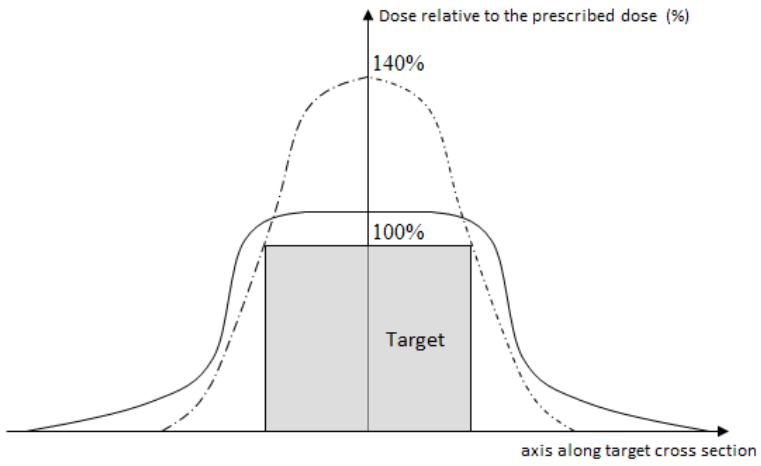

Fig. 3. Dose profiles across the target between conventional (—) and hypofractionated dose fractionation plans (- -).

HRT presents different dose distribution requirements, and different planning techniques must be implemented. Unfortunately, the increasing quantity and complexity of beam arrangements make it an avalanche of time and effort; the optimization process becomes highly complicated, inefficient and the results could be suboptimal. Only when treatment planning techniques and processes are equipped to suit the special needs of hypofractionated treatment planning will clinicians be able to design optimized treatment plans within the practical resources constraints. The aim of the first part of this study is to determine a relation between the incidence of normal lung toxicity and the dose distribution for hypofractionated lung patients.

1.4.3 Investigation on a newly developed planning technique

Characteristics of a HRT planning treatment include: high degree of conformality of prescription isodose lines, enclosure of inhomogeneities and highest isodose lines inside the target and rapid dose fall off outside the target. IMRT offers the ability to spare normal tissues surrounding tumors while delivering a tailored and conformal prescribed dose to a target. Linac based IMRT can be delivered with either segmental IMRT (sIMRT) or dynamic IMRT (dIMRT). The IMRT delivery technique in this study used a multi-leaf collimator (MLC) and fixed gantry positions. In this context, there are two main methods for dose delivery: sIMRT, also referred to as step-and-shoot technique, using a superposition of MLC segments, and the so called sliding window technique, also referred as dynamic IMRT using an open field strip defined by the MLC and moving across the field width. Both methods have different shortcomings; in the case of dIMRT, the beam is on during the entire dose delivery leading to an increased number of monitor units (MUs)[54], which increases leakage radiation through MLC therefore increasing adverse exposure to the patient[55]. Depending on the treatment energy, IMRT treatments require up to 4.9 more MUs than conventional treatments, thus increasing the risk of secondary malignancies from 1.7% for conventional treatments to 2.1% and 5.1% for IMRT treatments

using respectively 10 MV and 18 MV x-rays[56]. In the case of sIMRT delivery, a high number of segments will increase the treatment delivery time thus increasing the risk for the patient of moving during a prolonged treatment. Can IMRT be used in the case of lung hypofractionated radiation therapy?

In comparison with other treatment sites, a tumor in the lungs, because of its movement, presents a dual challenge in target delineation and localization. In addition, when treating a moving target with IMRT, there is an intrafractional organ motion effect due to the interplay between the motion of the leaves and the target thus causing a dosimetric blurring effect. Several authors have investigated this subject[57-60], and they all concluded that the interplay between organ motion and leaf motion is not dosimetrically significant for fractionated radiation therapy delivered over thirty fractions. However, we are considering hypofractioned lung treatment delivered over three to five fractions; hence the dosimetric effect cannot be considered insignificant anymore. In this case, reducing IMRT plan complexity would be beneficial. How then can we reduce IMRT plan complexity?

Traditionally the IMRT optimization process is a two-step process; optimized fluence patterns are converted into deliverable MLC segments via a leaf sequencer. The quality of a plan depends intrinsically on its leaf sequencing algorithm. Researchers have been working on improving efficiency of leaf sequencers[61]. However, controlling the complexity of a leaf sequencer often leads to deterioration in plan quality compared to original optimum fluence pattern[62]. A one-step process, direct aperture optimization (DAO) has been proposed and developed. DAO directly optimizes the beam weights, jaw and leaf positions. Parameters such as the minimum segments area as well as the maximum number of segments can be controlled. The feasibility and potential advantages of DAO over the traditional two-step IMRT optimization has been shown [63].

Dvorak *et al.*[64] reported on the impact of leaf width and the efficiency of IMRT for lung and liver HRT, and concluded in their study that standard hypofractioned radiation therapy treatment techniques, like stereotactic body radiation therapy (SBRT), could not be improved by IMRT approaches. First, the maximum number of segments per beam in their study, 15, was set too high for a stereotactic treatment approach, and secondly the treatment planning system used in the study applied a pencil beam algorithm during IMRT optimization, and a collapsed cone convolution algorithm for the final dose computation. In regions of large density inhomogeneities, it has been shown that, unlike the collapse cone convolution algorithm, the pencil beam algorithm, although fast, was not accurate enough [65-66]. Can we then use a DAO algorithm for planning of lung HRT? And if so, can we considerably reduce the plan complexity and the number of segments while improving dosimetric parameters?

A complex IMRT plan, with a high degree of dose modulation, requires more segments and more MUs[55]. Craft *et al.*[67] showed that the number of MUs can be reduced in an IMRT plan without depreciating the plan quality. Jiang *et al.*[68] showed that a minimum of 5 MLC segments per beam are necessary to achieve acceptable IMRT plans. Can we expand that conclusion and treat lung lesions with hypofractioned dose regimen using IMRT-DAO optimization and less than 5-segments per beam?

In this study we are using a DAO algorithm, the direct machine parameter optimization (DMPO) algorithm (Raysearch Laboratories AB, Stockholm, Sweden) implemented on the ADAC Pinnacle (Pinnacle3, Philips Medical Systems, Andover, MA) treatment planning system. Our approach was to use the DMPO algorithm to reduce plan complexity allowing successively one and five segments per beam angle. The goal of the second part of this study is to investigate the potential benefits of beams optimized with DMPO with one large segment per beam for

oligometastatic lung HRT and compare them with standard plan optimized with 5-segments per beam and with traditional 3DCRT plans.

1.4.4 Hypofractionated image guided radiation therapy (HIGRT)

An ideal HRT plan delivers more dose to the tumor and less dose to the normal tissue. This feature presents new challenges in almost all aspects of a treatment, including the immobilization of the patient during simulation and delivery, the localization of the target in treatment planning, and the management of respiratory motion and other organ motions. Respiratory motion is a significant source of geometric uncertainties. In radiation therapy, organ motion due to breathing are accounted for in the design of the internal target volume (ITV) [69], which consists of gross target volume (GTV) and clinical disease volume plus margin to account for breathing motion uncertainties. Margins for setup uncertainties are added to the ITV to design the planning target volume (PTV). Reducing the influence of organ motion can reduce the size of the PTV, hence decreasing the beam size, and consequently reducing the amount of lung exposed to radiation.

Advancement in imaging technologies have been used to better and more frequently acquire images of a patient throughout his radiation treatment. Over the last decade, image guide radiation therapy (IGRT) has emerged as a strategy to manage organ motion and patient set-up verification. IGRT strategies can be described as: computed tomography (CT) scanning data acquisition management, patient breathing control management, as well as set-up and geometrical verification.

CT scanning data acquisition management

An optimum target definition depends on the CT data acquisition. Tumor contours and breathing patterns vary from patient to patient, and individualized patient-based margins are needed for precise target definition [70-71]. CT scanners create thin section planar images of the patient, a motorized table moves through the circular opening of the CT imaging system, where an x-ray source and detectors rotate around the patient. The challenge is due to the interplay of tumor and couch motion. Several techniques have been used to account for this issue, including using multiple scans, one at each extreme phase of the breathing cycle, end-expiration and end-inspiration[72], slow CT scans have also been used[73], and more recently 4D-CT[74-79] scans have been used for target delineation. 4D-CT scan consists of respiration-correlated CT scanning where the patient breathing cycle is divided up in phases (e.g., 10 phases) and each scan is registered to its corresponding breathing cycle phase.

Patient breathing control management

Several methods exist to manage patient breathing such as breath-hold or breathing control methods[80-82] delivering radiation during a breath hold, abdominal compression[83-84] forcing shallow breathing with a pressure plate against the abdomen, and respiratory gating [85-87]. Respiratory gating is the least intrusive of all these methods. There have been numerous studies of respiratory gating both internal and external. Keall *et al.*[88] showed that respiratory gating can significantly reduce breathing-motion margins, Shirato *et al.*[89] described the physical aspects of internal markers using fluoroscopic tumor tracking. In 2006 Fang *et al.*[90] published a retrospective analysis of early stage NSCLC patients to assess the outcomes of 3DCRT and two-dimensional (2D) planning, they showed that patients treated with external respiratory gating are four times more likely to survive than those not treated with respiratory gating; suggesting that

managing respiratory motion via respiratory gating might improve survival in lung cancer patients. During respiratory gating, it has been demonstrated that tumor position is most reproducible in the vicinity of the end-exhale breathing phase[91], therefore the gated window is often centered at the normal respiratory pause at end exhalation.

Set-up and geometrical verification

Finally set-up and geometrical verification has also evolved and offer accurate and effective tools to target and track tumors. The Varian On-Board Imager (OBI) used in our study integrates a kilovoltage (kV) x-ray source and a large flat panel detector. Two robotic arms are mounted on the treatment machine gantry, which can be quickly and automatically retracted out of the way when not in use. The kV imaging system operates in a plane orthogonal to the megavoltage treatment beam. Two orthogonal kV images, typically lateral and AP radiographs, are acquired by rotating the gantry 90°. The AP and lateral kV radiographs are matched with referenced images to reproduce the isocenter position. Referenced images are usually digitally reconstructed radiographs (DRR) obtained from the CT data set used in treatment planning. Using bony structures such as vertebral bodies, vertebral processes, vertebral spaces, and ribs delineated on the planning DRR, the matched image sets are overlaid and shifted until a match is accepted by the physician. The result from this 2D/2D anatomical matching is a computed offset with usually three degrees of freedom, x, y, and z translations. The treatment couch is then repositioned according to the obtained shifts. For all patients treated, patient position is verified before online correction. In addition to 2D/2D matches, the OBI system also allows volumetric verification, 3D/3D matching. With a single gantry rotation, and 3D volumetric CT data set is reconstructed while the patient and treatment couch remain stationary. The acquired cone beam CT (CBCT) is then matched with the reference planning CT. Similarly to the 2D/2D match

process, the reconstructed CBCT is registered with the planning CT in the 3D/3D match application by the physician. Bony structures as well as soft tissue details are used to verify patient and tumor positions. Figure 4 shows an example of 3D/3D data set registration.

Early SBRT studies used a body frame, a rigid patient immobilization device with a stereotactic coordinate system for pre-treatment imaging and treatment planning. The immobilization system also included abdominal compression to limit diaphragm motion thus limiting the tumor motion due to breathing. Figure 5 shows an example of an Elekta stereotactic body frame.

Studies using the Elekta body frame achieved setup errors of approximately 3 to 4 mm in all directions [92-93]. Other studies showed that an approach with OBI coupled with a standard immobilization device, such as Alpha Cradle (Smithers Medical Products, North Canton, USA) shown in Fig. 6 could detect residual setup variations of approximately 3 to 5 mm[94-95].

In the beginning and in the absence of image guidance, the stereotactic body frame was an integral part of SBRT. With the improvement of image-guided radiation therapy there was less need for the stereotactic frame. The radiation oncology team still needs to be very conscientious of immobilization but does not need to rely on a stereotactic coordinate system anymore. In the present study we are using a standard Alpha Cradle for patient immobilization coupled with an IGRT approach with 4D-CT simulation, kV radiographs and CBCT. In the following sections of this study, we will refer to HIGRT when specifically referring to the technique described above. Similarly the term lungs will always refer to the normal lung tissue composed of the whole lungs minus the GTV.

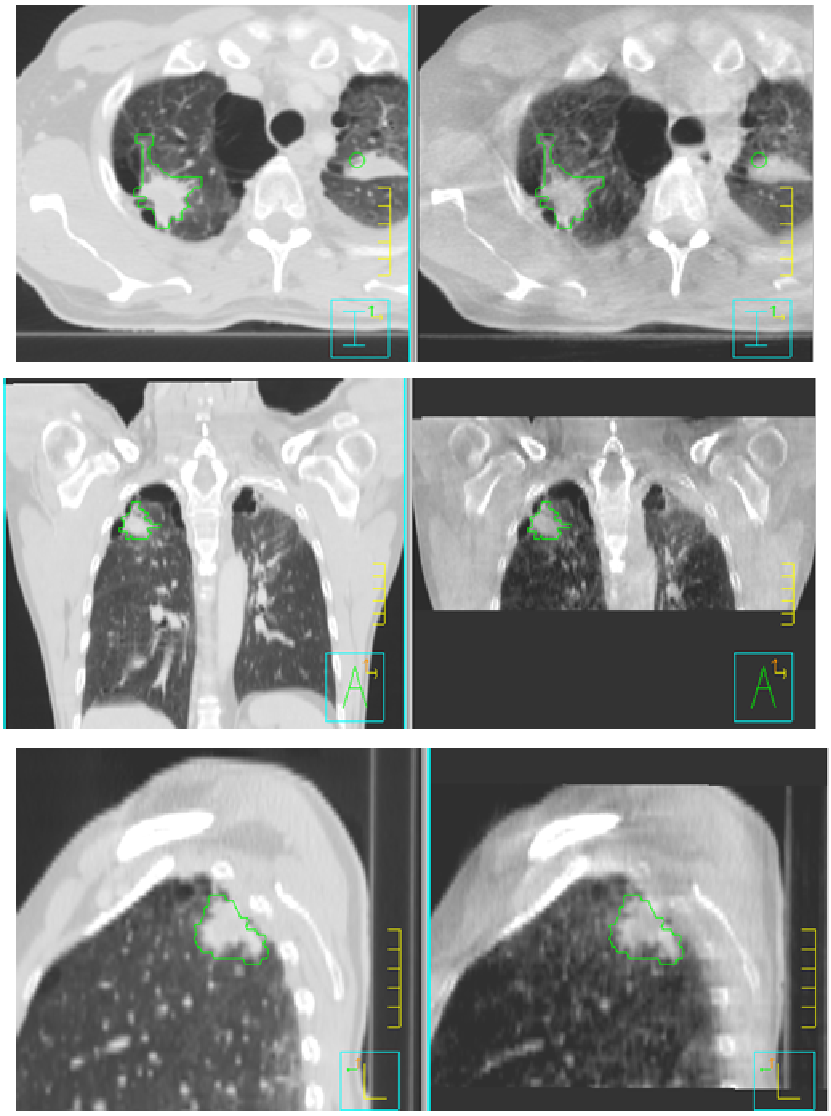

Fig. 4. Axial, coronal and sagital views of a patient treated with HRT to a lesion in the lung delineated in green. 3D/3D registration of the planning CT data set (left) and the CBCT (right) acquired before treatment shows adequate and optimum patient and tumor localization and positioning

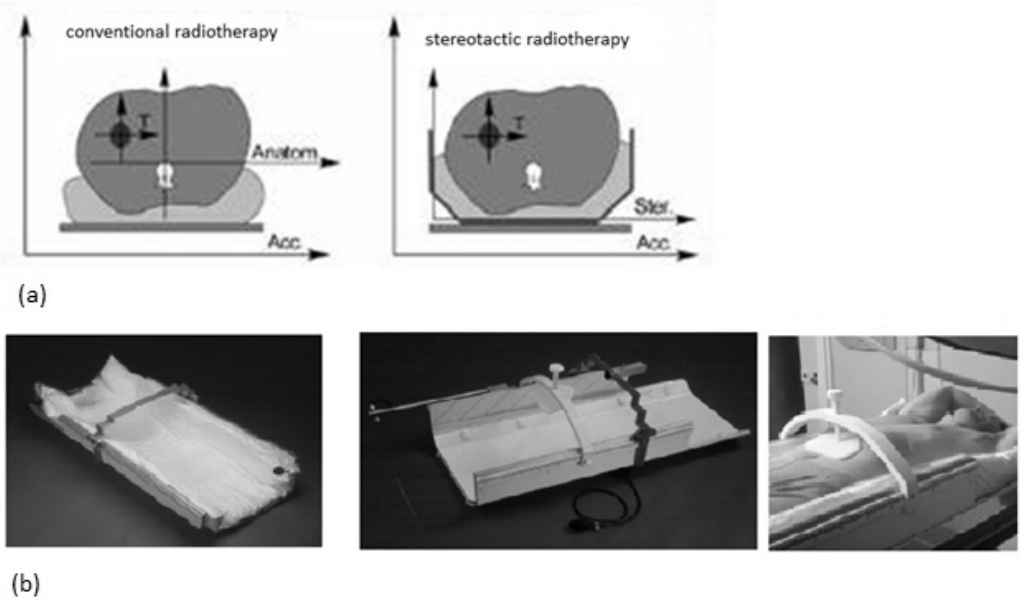

Fig. 5. (a) Diagram of coordinate systems used in conventional radiotherapy (left) and stereotactic body radiotherapy (right). (b) Example of an Elekta body frame.

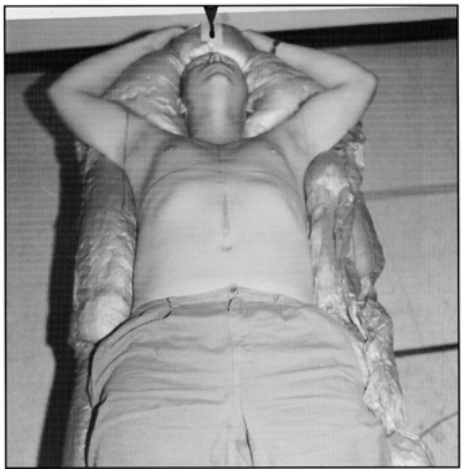

Fig. 6. Smithers Alpha Cradle (Smithers Medical Products, North Canton, USA) immobilization device

1.4.5 Quality assurance (QA)

With the elevated expectation of tumor local control and adjacent normal tissue sparing, the accuracy and precision of dose delivery becomes extremely critical for the hypofractionated radiation therapy. Although numerous methods have been applied to minimize the geometric error in aligning target with radiation, and extensive QA programs have been developed to maintain the accuracy, the natural respiratory motion of patients presents a special challenge for radiation therapy on targets in the lungs. For conventional therapy, the dosimetric errors resulted from irradiating a moving target with a static beam are considered to be insignificant because the large number of fractions and the random nature of breathing may smear out the errors. However, these errors may noticeably modify the dose distribution in HRT where only few fractions are used and rigorous patient breathing control and monitoring techniques are employed. The deviation of dose delivered could result in severe tumor under-dose and normal tissue over-dose. With the increasing number of conformal beams, the possibility and the magnitude of dose deviation may increase significantly. In addition, when a new planning technique/process is implemented, the deliverability of resulting treatment plans must be verified and the deviation of delivered dose from planned dose must be fully assessed. Then, clinicians will have the confidence that the optimized treatment plan is accurately delivered and the benefit of hypofractionation can be realized.

1.5 A proposal to improve the implementation of HRT

Compared to conventional radiation therapy, dose-hypofractionated therapy is a new treatment paradigm. As discussed in the previous section, some major challenges have been identified in the clinical implementation of this type of therapy. This dissertation proposes to improve the clinical implementation of HRT for lung malignancies in three aspects: first of all,

dosimetric end-points to guide plan optimization and evaluation will be investigated; secondly, a new planning process will be improvised to facilitate the design of a complex radiation treatment plan; finally, a dose verification method will be developed in the context of measuring radiation doses on moving targets for complicated plans including multiple small fields. The roadmap of the study is outlined below:

Aim 1: Determine the relation between the incidence of normal lung toxicity and the dose distribution for HRT for patients with multiple metastases in the lungs.

-select patients with lesions in the lung and treated with hypofractionated dose regimen

-evaluate lung toxicities for each patient using the National Cancer Institute Common Terminology Criteria (NCI-CTC) for Adverse Events[96].

-analyze the dose distribution calculated for the normal lung tissue

Aim 2: Develop a novel radiation planning method for lung patients treated with HRT to multiple metastases in the lungs and compare it with other planning techniques

-select patients whose treatments were previously planned using a conventional 3D conventional radiation therapy (3DCRT) method to multiple lesions in the lungs, and retrospectively re-plan them with the newly developed radiation planning technique

-define the dosimetric endpoints for the intercomparison study

-compare and analyze isodose dosimetric endpoints among the different planning techniques

Aim 3: Verify and validate the planning technique presented in Aim 2 via dosimetric quality assurance (QA) delivered on a motion phantom.

-deliver the optimized beams on a motion phantom

-evaluate the dose in the lung, the target and at the edge of the target

-compare dose measurements with calculated doses

2. AIM 1: DETERMINE THE RELATION BETWEEN THE INCIDENCE OF NORMAL LUNG TOXICITY AND THE DOSE DISTRIBUTION FOR HYPOFRACTIONATED LUNG PATIENTS

2.1 Materials and methods

2.1.1 Study object

The study object consisted of patients with multiple metastases in the lungs. Patients with 1 to 4 sites of metastatic cancer received doses of radiation to all known sites of cancer with HIGRT. Twenty-eight patients with 51 lesions in the lung were evaluated for this study. The median combined PTV was 81.37 cm^3, with a minimum of 13.63 cm^3 and a maximum of 265.60 cm^3. All patients underwent CT-based treatment planning in custom-made immobilization with image guided techniques as described in the previous section, and received 24 Gy to 48 Gy in 3 fractions. The dose cohorts are described in Table II. In addition, one patient in the study received a dose of 50 Gy in ten fractions and another one 60 Gy in thirty fractions to one of their lung sites, respectively. Dose was prescribed to the PTV edges and to the 80%-90% isodose line, with 95% of the PTV required to receive 95% of the prescription dose. The three radiation therapy fractions were separated by 2 to 8 days. Tumor characteristics of the study object are described in Table III.

Table. II. Description of dose cohorts in the study

Dose cohort	Number of patients	Number of lesions
8Gyx3	8	12
10Gyx3	8	8
12Gyx3	8	11
14Gyx3	10	13
16Gyx3	3	4

Table. III. Metastases locations sorted by their number of treated lesions; RLL: right lower lobe, RUL: right upper lobe, RML: right medial lobe, LUL: left upper lobe, LLL: left lower lobe, LML: left medial lobe.

Patient ID#	Primary tumor	Number of treated lesions	Metastases locations in lung	PTVs volume (cc)	Whole lungs minus GTV volume (cc)
1	Melanoma	4	RLL, RUL, LUL, RML	58.16, 8.22	2479.89
2	Head and Neck	4	LML, LML ant, LML post, LLL	197.99	3087.82
3	Colon	3	RUL, RLL, LUL	50.02, 60.10	2624.19
4	Colon	3	RUL, RLL, LUL	45.20, 52.50, 88.65	2022.46
5	Parotid	3	LL, RLL, RUL	19.10, 21.35	3084.39
6	Lung	3	RUL, RML, RLL	81.20, 33.80, 89.90	4798.63
7	Sarcoma	2	RML, RLL	19.50, 145	2380.00
8	Lung	2	LUL ant, LUL post	40.3, 114.4	2795.80
9	Renal cell	2	RLL, RML	27.80, 43.20	2168.71
10	Lung	2	RUL, RLL	5.7, 52.50	4206.61
11	Thyroid	2	RUL, LUL	28.6, 8.6	2936.34
12	Lung	2	RUL, LUL	21.00, 59.80	2721.87
13	Uterus	2	RUL, LUL	15.72	2362.84
14	Lung	2	RML, RUL	189.67	6078.88
15	Glottis	2	LML, LLL	37.11	6110.61
16	Small bowell	1	LUL	148.35	2731.66
17	Lung	1	RUL	179.01	2420.02
18	Head and Neck	1	RUL	81.94	3791.17
19	Ovarian	1	RLL	205.86	1808.01
20	Lung	1	RUL	248.26	1543.17
21	Colon	1	RLL	13.63	2023.37
22	Lung	1	LML	27.17	2000.75
23	Lung	1	LML	133.9	2649.00
24	Rectum	1	LLL	19.78	2507.44
25	Renal cell	1	RML	265.6	3427.09
26	Head and Neck	1	RUL	60.86	2843.60
27	Breast	1	RUL	36.52	3785.88
28	Renal cell	1	RUL	72.26	2299.66

2.1.2 Toxicity and dosimetric analysis

Patients were evaluated after treatment and toxicities were scored using the NCI-CTC[96] scoring for acute and late toxicities. Grade 1 toxicities were associated with radiographic changes in less than 25% and no symptoms, Grade 2 toxicities were associated with symptomatic cough with narcotics indicated, and radiographic changes (fibrosis) in 25 to 50% of the lungs. Grade 3 toxicities were associated with symptomatic cough requiring oxygen, and radiographic changes of 50 to 75% of fibrotic lungs.

For each patient we looked at lung metrics using the dose volume histogram (DVH). In the case of non-uniform dose, we needed to use DVH reduction method to convert a heterogeneous dose distribution into a uniform dose distribution. The volume of the organ was divided into sub-volumes where v_i was the fraction of volume receiving a total dose D_i. The dose bin sizes were chosen small enough to consider the dose uniform in each sub-volume. The (v_i, D_i) were obtained from the DVH for each patient and for the total lungs excluding the GTV. We computed from the DVH the MLD, the V20 and V13, representing the percentage of lungs receiving 20 Gy or more and 13 Gy or more, respectively.

In addition, since we were dealing with various dose schemes, we could not simply compare lung metrics to come up with dose guidelines. We used another DVH reduction method[18] to convert the dose D_i in each sub-volume v_i from a hypofractionation regimen into a standard fractionation with a reference dose d_{ref} of 2 Gy. For each patient we computed the mean MLD and NTD as described below:

$$MLD = \left(\sum_i v_i D_i \right) \quad . \quad (4)$$

$$NTD_i = D_i \frac{\left(1 + \frac{d_i}{\alpha/\beta} \right)}{\left(1 + \frac{d_{ref}}{\alpha/\beta} \right)} . \ (5) \ , \ NTD = \left(\sum_i v_i NTD_i \right) \quad . \quad (6)$$

with $D_i = n * d_i$, n is the total number of fractions, $d_{ref} = 2\,\text{Gy}$ and $\alpha/\beta = 3\,\text{Gy}$.

We also estimated the risk of radiation pneumonitis, also called the normal tissue complication probability (NTCP) using the method developed by Mohan *et al.*[97], and based on the Lyman[98]-Kutcher-Burman[99] (LKB) model.

$$NTCP = \frac{1}{\sqrt{2\pi}} \int_{-\infty}^{t} e^{-\frac{x^2}{2}} dx \ . \ (7)$$

$$t = \frac{NTD - TD_{50}}{mTD_{50}} \quad . \quad (8)$$

where t is an intermediate variable used to compute the NTCP, TD50 is the uniform dose to the entire organ resulting in a 50% complication risk, RP, and m is a measure of the slope of the sigmoid curve.

Regarding the statistical analysis, we performed a maximum likelihood fit of the NTCP model to our data to obtain the best fit parameters, TD50 and m, for our study, given the outcome of each individual.

For each patient we scored the incidence of RP of Grade ≥ 2 with 1 and 0 otherwise. We then divided patients into 4 subgroups according to their NTD, and reported the incidence of RP

of Grade ≥ 2 for each subgroup. The two parameters of the NTCP model, were fitted by means of maximizing the logarithm of the likelihood function described below:

$$\ln(L) = \sum_{i}^{n} \left[ep_i \ln(NTCP_i) + (1 - ep_i)(1 - \ln(NTCP_i)) \right]. \quad (9)$$

where n is the number of patients, and ep_i is the binary outcome for occurrence of RP of Grade≥ 2. The 95% confidence interval (CI) around the maximum likelihood estimation was calculated for TD50 and m. All calculations were performed using the Stata Data Analysis Software (StataCorp, College Station, TX). A two-tailed p value less then 0.05 was considered statistically significant.

2.2 Results

Summary of patients showing Grade ≥ 2 and Grade ≤ 1 toxicity is shown in Table IV. Eight patients experienced Grade ≥ 2 toxicity, five with Grade 3 and three with Grade 2 toxicity.

The summary of the p values for the lung and PTV metrics is shown in Table V. The volume of the whole lungs was shown to be a significant indicator for RP of Grade ≥ 2, as well as the lung metrics V13, V20, MLD and NTD with p values below 0.05. Grade ≥ 2 and Grade ≤ 1 group had a median V13 of 18.78 % and 11.63 %, respectively; Grade ≥ 2 and Grade ≤ 1 group had a median V20 of 12.40 % and 6.23 %, respectively, Grade ≥ 2 and Grade ≤ 1 group had a median MLD of 787.75 cGy and 498.45 cGy, respectively, finally Grade ≥ 2 and Grade ≤ 1 group had a median lungs volume of 2540.26 cm^3 and 3168.36 cm^3, respectively. The PTV volume was not a significant predictor for RP Grade ≥ 2 (p=0.5516).

Table VI shows the percentage of primary tumor origin for both subgroups of patients experiencing toxicities of Grade ≥ 2 and Grade ≤ 1.

Table. IV. Summary of patients showing Grade ≥ 2 and Grade ≤ 1 toxicity.

Patient ID#	Number of treated lesions	Dose prescriptions	PTVs volume (cc)	Lungs volume (cc)
		RP Grade ≥ 2		
1	4	12Gyx3, 12Gyx3, 12Gyx3, 10Gyx3	66.380	2479.89
16	1	12Gyx3	148.35	2731.66
12	2	12Gyx3, 14Gyx3	80.80	2721.87
7	1	14Gyx3, 2Gyx30	164.50	2380.00
8	2	14Gyx3, 5Gyx10	154.70	2795.77
17	1	10Gyx3	179.01	2420.02
3	3	14Gyx3, 14Gyx3, 10Gyx3	110.12	2624.19
9	2	16Gyx3, 8Gyx3	71.00	2168.71
		RP Grade ≤ 1		
10	2	10Gyx3, 8Gyx3	58.20	4206.61
18	1	12Gyx3	81.94	3791.17
19	1	12Gyx3	205.86	1808.01
20	1	8Gyx3	248.26	1543.17
4	3	8Gyx3, 16Gyx3, 10Gyx3	186.35	2022.46
11	2	16Gyx3, 16Gyx3	37.20	2936.34
21	1	14Gyx3	13.63	2023.37
5	3	14Gyx3, 14Gyx3, 16Gyx3	40.45	3084.39
2	4	8Gyx3, 8Gyx3, 8Gyx3, 8Gyx3	197.99	3087.39
13	2	8Gyx3, 8Gyx3	15.72	2362.84
22	1	10Gyx3	27.17	2000.75
23	1	14Gyx3	133.90	2649.00
24	1	12Gyx3	19.78	2507.44
25	1	10Gyx3	265.60	3427.09
26	1	10Gyx3	60.86	2843.60
27	1	8Gyx3	36.52	3785.88
28	1	14Gyx3	72.26	2299.66
14	2	14Gyx3, 14Gyx3	189.67	6078.87
15	2	12Gyx3, 12Gyx3	37.11	6110.61
6	3	8Gyx3, 12Gyx3, 14Gyx3	204.90	4798.63

Table. V. Summary of the p values for the lungs and PTV metrics

Lungs		RP Grade ≥ 2	RP Grade ≤ 1	p values Grade ≥ 2 vs Grade ≤ 1
V13 (%)	Mean	18.7800	11.6300	0.0447
	St Dev	7.1500	7.2500	
	median(min-max)	19.95(11.06-26.02)	12.65(4.02-19.87)	
V20 (%)	Mean	12.4013	6.2300	0.0235
	St Dev	5.9719	4.2163	
	median(min-max)	11.10(6.3-24.2)	6.74(1.14-13.88)	
MLD (cGy)	Mean	787.75	498.4500	0.0218
	St Dev	269.38	244.6287	
	median(min-max)	752.50-(498.00-1235.00)	433(205-1117.00)	
NTD(2Gy) (cGy)	Mean	1449.94	874.3492	0.0069
	St Dev	413.91	511.8820	
	median(min-max)	1504(917-1912)	724(256.27-2125.90)	
Volume (cc)	Mean	2540.2640	3168.36	0.0499
	St Dev	215.0704	1307.11	
	median(min-max)	2552.04(2168.70-2795.77)	2889.97(1543.17-6110.61)	

PTV		RP Grade ≥ 2	RP Grade ≤ 1	p values Grade ≥ 2 vs Grade ≤ 1
Volume (cc)	Mean	121.8575	106.6685	0.5516
	St Dev	45.2817	86.7925	
	median(min-max)	129.23(66.38-179.01)	66.56(13.63-265.60)	

Table. VI. Origin of oligometastasis for the two subgroups of patients experiencing RP Grade ≥ 2 and RP Grade ≤ 1

Primary tumor	Percentage of patients with RP Grade ≥ 2	Percentage of patients with RP Grade ≤ 1
Melanoma	12.5%	0.0%
Breast	0.0%	5.0%
Colon	12.5%	10.0%
Glottis	0.0%	5.0%
Heand and Neck	0.0%	15.0%
Lung	37.5%	30.0%
Ovarian	0.0%	5.0%
Parotid	0.0%	5.0%
Rectum	0.0%	5.0%
Renal cell	12.5%	10.0%
Sarcoma	12.5%	0.0%
Small bowel	12.5%	0.0%
Thyroid	0.0%	5.0%
Uterus	0.0%	5.0%

We plotted the MLD vs NTD for each patient (Fig. 7) and we could observe a nearly linear relationship with the NTD being equal to 1.8 times the MLD.

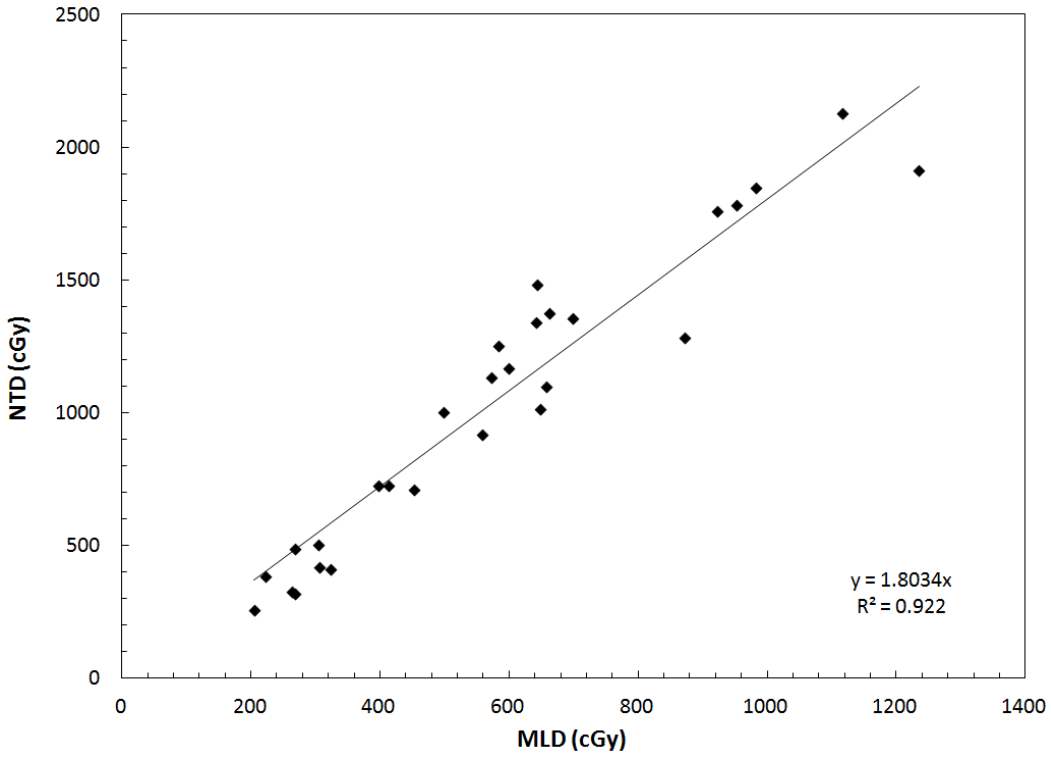

Fig. 7. NTD plotted as a function of MLD with linear regression modeling their relationship

In addition, we computed the crude incidence of RP Grade ≥ 2, and binned them by doses of 450 cGy (Fig. 8). In the first patient bin of NTD doses from 0 to 550 cGy, zero out of eight patients experienced toxicity; in the second patient bin of NTD doses from 551 to 1013 cGy, two out of six patients experienced toxicity RP Grade ≥ 2; in the third patient bin of NTD doses from 1014 to 1355 cGy, two out of seven patients experienced toxicity RP Grade ≥ 2; and

finally in the fourth patient bin of NTD doses from 1354 cGy and above, four out of seven patients experienced toxicity RP Grade ≥ 2. Error bars represent the 68% CI of the observed incidence.

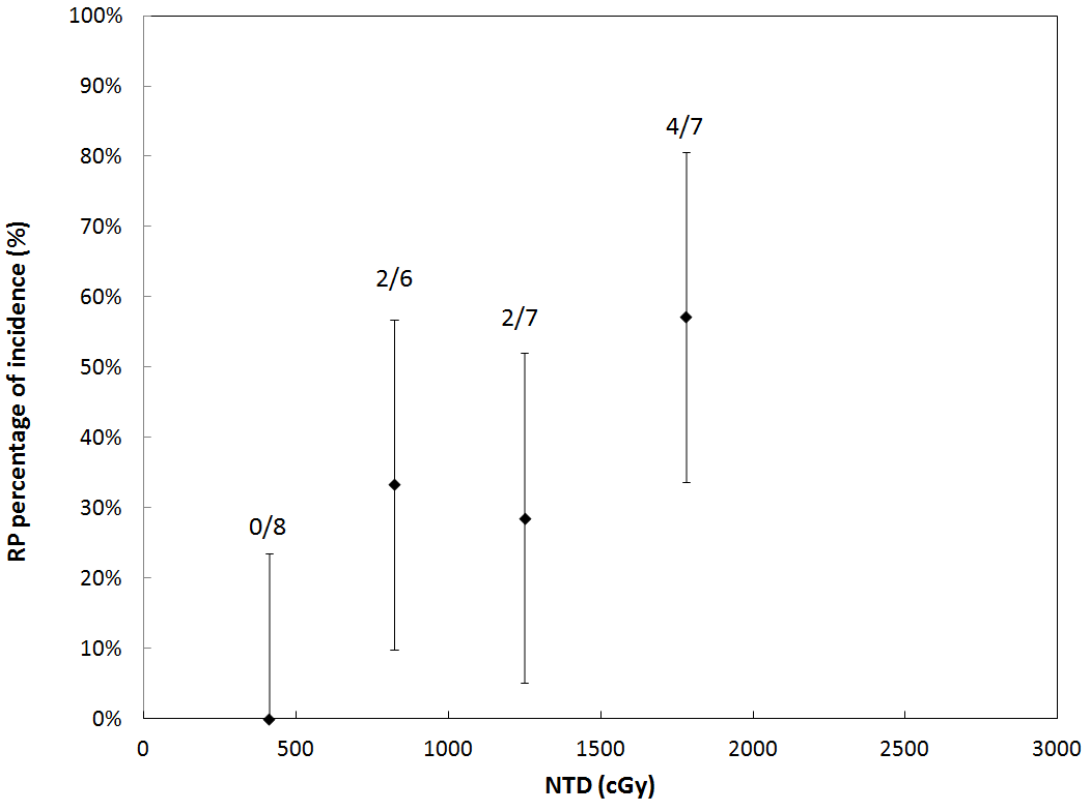

Fig. 8. Observed incidences of RP Grade ≥ 2. Error bars shows the 68% confidence interval (CI)

The two parameter fit that was equal to the observed model resulted in a TD50 of 1550 cGy, with 1170-2740 cGy, 95% CI, and an m value of 0.44, with 0.26-1.07, 95% CI (Fig. 9).

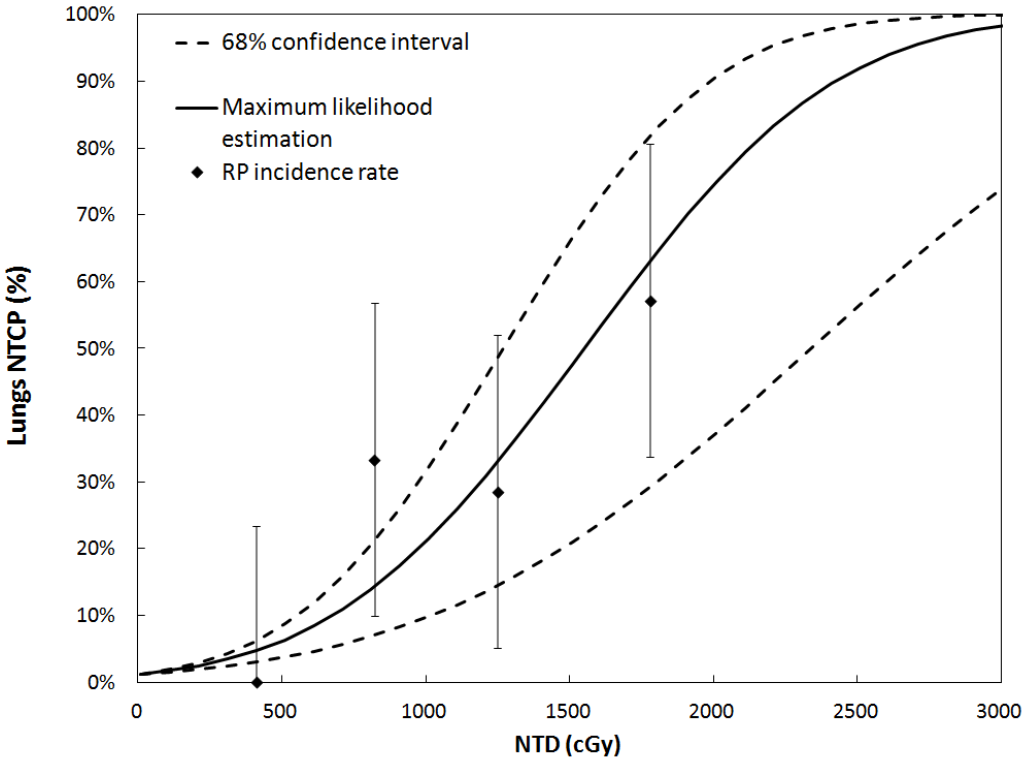

Fig. 9. Maximum likelihood estimation of NTCP plotted as a function of NTD (-), and 68% confidence interval of NTCP plotted as a function of NTD (--)

2.3 Discussion

In contrast to conventional therapy where there is abundant and practical data for making proper clinical decisions, the experience on HIGRT is more limited. There is no well-established or clinically-proven standard for treatment planning. Although treatment plans were usually conservative for the sake of patient safety, more clinical data must be collected and analyzed. In particular, the MLD and the V20 are the two most important dosimetric endpoints in predicting incidence of RP in conventional therapy[100]. Other metrics such as the V13 have also been shown to correlate with the risk of RP[101-104]. The applicability of these RP predictors in hypofractionated dose schemes needs to be investigated and the dosimetric endpoints that provide the most predictive power remain to be determined. The first specific aim of this study is to determine a relation between the incidence of normal lung toxicity and the dose distribution for hypofractionated lung patients.

We use the NCI-CTC for Adverse Events scoring system to report the incidence of RP Grade ≥ 2. We observed a 28% crude incidence of RP Grade ≥ 2.

Investigators[52] have shown that a relationship between PTV size and the incidence of RP might exist; however in our study PTV, volume was not a significant predictor for the incidence of RP ($p=0.5516$). We can explain this difference by the fact that more than half of the patients in our study had multiple metastases in the lungs and when treating two or more lesions in the lungs the PTV volume may not be a good enough predictor for RP.

The V20 and V13 were significant predictors of RP Grade ≥ 2. The V20 was a more significant predictor ($p=0.0235$) compared to V13 ($p=0.0447$) which might suggest that higher doses might contribute more to the incidence of RP compared to lower doses; hence suggesting that high doses to a small volume of normal lung tissue is most important for lung toxicity over low doses to a large volume. This conclusion is inconsistent with experiments on rats by

Semenenko *et al.*[105] where larger volumes of lungs exposed to lower doses induced more toxicities than smaller volumes of lungs exposed to higher dose. It is important to note that the endpoint in their study was the breathing rate as opposed to RP, and that lung functionalities between the rat model and the human might differ as well, and could explain the observed discrepancies.

Patients with RP Grade ≤ 1 had significantly larger lung volume with a median of 3168.36 cm^3 versus 2540.26 cm^3 for patients with RP Grade ≥ 2, since we are delivering radiation therapy to one to four targets in the lungs, a larger overall lung volume will demonstrate a lower mean dose.

Similar to other studies [106] [107], we found the MLD to be a significant predictor for RP Grade ≥ 2 in our study. Borst *et al.*[106] looked at RP incidence in 128 patients treated with lung HRT and also found significant relationship between MLD and RP incidence. They observed a median MLD of 640 cGy and we observed a median of 752.2 cGy in patients with RP Grade ≥ 2 versus 433 cGy for patients with RP Grade ≤ 1. However, since we were dealing with multiple dose regimens, we needed to account for these differences using the NTD.

An important finding in this study was that NTD predicted most significantly RP Grade ≥ 2 (p=0.0069). It is important to point out that the NTD formula is directly derived from the LQ formalism and it is debated in the literature whether this model is still valid in HRT [108-109]. Borst *et al.*[106] evaluated the relationship between MLD and RP incidence after lung SBRT and conventional fractionated RT. Using the LQ formalism, with NTD corrected to 2 Gy fractions for SBRT and MLD for conventional fractionated RT, they showed no significant differences between each dose response. Other authors[110-112] reported on a dose-response relationship in SBRT between tumor control probability and BED, which is also derived from the LQ formalism. Opponents of the LQ model at high dose per fraction report that if the model

correctly describes the log cell survival at low dose, the log cell survival becomes linear at high dose[113 114], and therefore the LQ model might overestimate the cell survival. Investigators proposed a modified LQ model to account for the linearity of cell survival at high dose per fraction. Park *et al.*[114] proposed the LQ(L) model, a linear-quadratic model at low dose and linear model at high doses with a transition dose d_t, designed to better describe cell survival for HRT. Borst *et al.*[115] evaluated the NTCP fit predicting RP, using the LQ model and the LQ(L) for 128 patients treated with HRT to the lung. They concluded that the LQ model was the best method for converting physical dose to NTD to predict RP. Consequently, results from other studies and data from the literature support the use of LQ formalism and NTD in HRT as a possible RP predictor. Although some studies may confirm the use of the LQ model in HRT, further investigation is still needed to fully validate it in hypofractionation.

We evaluated the parameters of the LKB model for our study, TD50 and m. We estimated a TD50 of 1550 cGy and an m value of 0.44. The recent study by Borst *et al.*[106] evaluated 128 patients for SBRT and estimated a TD50 of 1960 cGy, with 1600-3000 cGy 95% CI and m value of 0.43 with 0.33-0.59 95% CI. Their m value was very close to the one estimated in our study of 0.44. We observed more significant toxicity at lower dose level as indicated by our crude toxicity of 28% versus 11% for their study.

We used the DVH reduction model described above to compute the MLD and NTD. This model presents some limitations because it assumes for example that all regions of the lungs are of equal functional importance, while it has been shown that HRT to centrally located tumors can be significantly more toxic than other lung locations[26, 116]. In addition the lung is considered to be a parallel organ, with functional subunits called alveoli, which are thought to work independently and respond independently to radiation damage. However, with high dose per fraction this might no longer be true. Studies[117-118] have shown the existence of bystander effects

for lung cells exposed to radiation, and damaged alveolar cells might diffuse and cause damage to adjacent alveolar cells. Another example of the possible bystander effect of RP was illustrated in studies[119,120,121] showing that ipsilateral radiation therapy to lungs or breast tumors could induce RP to the contralatreal unexposed lung. Therefore, some particular areas of the lungs could act as serial structures in which a damage of a subunit may lead to the damage and loss of the entire group of subunits. A more robust and biologically weighted DVH reduction model might be needed to better evaluate radiation damages to lung tissues.

2.4 Conclusion

HIGRT for multiple metastases in the lungs requires careful evaluation of several lung DVH metrics including the MLD, V13 and V20. A dose-effect relation between NTD and RP for HIGRT treatments of multiple lung lesions may exist up to 48 Gy in three fractions as a predictor of lung toxicity. Also, the dose-response parameters derived in our study appear to agree with other hypofractionated results published in the literature. The dose-effect relationship needs to be further investigated in conjunction with analysis and development of the DVH reduction method to better model the temporal, as well as the spatial, distribution of radiation in the lungs during radiation therapy.

3. AIM 2: DEVELOP A NOVEL RADIATION PLANNING METHOD FOR LUNG PATIENTS TREATED WITH HRT

3.1 Materials and methods

3.1.1 Study object

Fifteen of the 28 oligometastasis patients studied previously were included in this retrospective study (ID#1 to 15). We selected all the patients who received HIGRT to multiple targets in the lungs. The reason for selecting this group was that the planning method for HIGRT can be tedious and cumbersome, especially in the case of multiple lesions since more normal lung is exposed to radiation. In addition among the 8 patients who had evidence of Grade 2 and above RP, 6 had 2 or more lesions in the lungs. The study object is presented in Table VII.

Since we were dealing with patients with several PTVs and dose prescriptions, we grouped for each patient the PTVs with the same dose prescription under one PTV. For each patient we took the union of the PTVs receiving the same dose and extracted data out of this union PTV. Volumes for each PTVs is shown in the study object table (Table VII)

In the study object, two patients (#7 and #8) received doses to PTVs with conventional dose fractionation in addition to the HIGRT treatment to a second PTV. We accounted for the dose from all the PTVs for these two patients.

Table. VII. Study object: multiple oligometastasis' locations

Patient ID#	Primary tumor	Number of treated	Metastases locations in lung	Dose prescriptions	PTVs volume (cc)	Whole lungs minus GTV
1	Melanoma	4	RLL, RUL, LUL, RML	12Gyx3, 12Gyx3, 12Gyx3, 10Gyx3	58.16, 8.22	2479.89
2	Head and Neck	4	LML, LML ant, LML post, LLL	8Gyx3, 8Gyx3, 8Gyx3, 8Gyx3	197.99	3087.82
3	Colon	3	RUL, RLL, LUL	14Gyx3, 14Gyx3, 10Gyx3	50.02, 60.10	2624.19
4	Colon	3	RUL, RLL, LUL	8Gyx3, 16Gyx3, 10Gyx3	45.20, 52.50, 88.65	2022.46
5	Parotid	3	LL, RLL, RUL	14Gyx3, 14Gyx3, 16Gyx3	19.10, 21.35	3084.39
6	Lung	3	RUL, RML, RLL	8Gyx3, 12Gyx3, 14Gyx3	81.20, 33.80, 89.90	4798.63
7	Sarcoma	2	RML, RLL	14Gyx3, 2Gyx30	19.50, 145	2380.00
8	Lung	2	LUL ant, LUL post	14Gyx3, 5Gyx10	40.3, 114.4	2795.80
9	Renal cell	2	RLL, RML	16Gyx3, 8Gyx3	27.80, 43.20	2168.71
10	Lung	2	RUL, RLL	10Gyx3, 8Gyx3	5.7, 52.50	4206.61
11	Thyroid	2	RUL, LUL	16Gyx3, 16Gyx3	28.6, 8.6	2936.34
12	Lung	2	RUL, LUL	12Gyx3, 14Gyx3	21.00, 59.80	2721.87
13	Uterus	2	RUL, LUL	8Gyx3, 8Gyx3	15.72	2362.84
14	Lung	2	RML, RUL	14Gyx3, 14Gyx3	189.67	6078.88
15	Glottis	2	LML, LLL	12Gyx3, 12Gyx3	37.11	6110.61

3.1.2 Study design

A retrospective planning study was developed to determine if the HIGRT planning process could be automated in the case of multiple lesions in the lungs. The primary objective was to determine if an inverse planning algorithm such as the DMPO optimization algorithm could be used while decreasing the number of segments per gantry angle. Jiang *et al.*[68] showed that a minimum of 5-segments per gantry angle were necessary to achieve acceptable step-and-shoot IMRT plans. New plans were generated for each of the cases in the study using the DMPO inverse planning algorithm allowing successively 1 and then 5-segments per gantry angle.

Each patient's actual treatment plan was restored from the archives. Typically, all were originally planned using non-coplanar 3DCRT treatment techniques. Each plan began with the selection and optimization of multiple (9 to 16) non-coplanar gantry positions. Beam aperture and weighting of 6 MV photons were manually and iteratively optimized to control the high dose gradient near serial critical structures and minimize low-dose spread to parallel organs. Dose calculations were performed using a commercial treatment-planning system (Pinnacle3, Philips Medical Systems, Andover, MA) via the convolution/superposition algorithm, including a full density heterogeneity correction. All plans were computed with a grid size of 3 mm.

To determine the benefit of inverse planning DMPO optimization, two new research plans were created for each patient in the study. These research plans used identical beam arrangements to the 3DCRT plan. However, beam aperture and weighting were optimized using the DMPO algorithm with static modulated 6 MV beams. DMPO parameters were set to allow 1 and 5-segments per beam for the 1-segment and 5-segments plans respectively. The optimization routine used the collapsed cone convolution dose calculation after ten successive iterations. Multiple iterative processes were necessary until the treatment planning goals were met.

In order to do an inter-plan comparison, all plans had the same PTV coverage, we normalized all plans so that the prescription isodose line covered 95% of the PTV.

3.1.3 Treatment plan evaluation

The conformality of the plans was evaluated using the conformality index R100 defined by the radiation therapy oncology group (RTOG)[122] and the more comprehensive conformality index CI proposed by Knoos *et al.*[123] which takes into account the degree of spatial intersection between the PTV volume and the isodose volume as defined below:

$$R100 = \frac{V_{\text{prescription isodose}}}{V_{PTV}} \quad (10), \qquad CI = \frac{V_{PTV}}{V_{TREATED}}. \quad (11)$$

where $V_{\text{prescription isodose}}$ is the volume of the prescription isodose line, $V_{TREATED}$ is the volume of the minimum isodose surrounding the PTV, and V_{PTV} is the volume of the PTV. The R100 value for an ideal plan is 1 and can go up to 2, the CI maximum and ideal value is 1 and can go as low as 0.3. High R100 scores means worse conformality, and a low CI score means worse conformality.

Additionally, we evaluated the sharpness of the dose gradient using the R50 index described in RTOG clinical trials and defined as the ratio of the 50% isodose line volume over the volume of the PTV. We also looked at the heterogeneity index (HI) defined as:

$$HI = \frac{D_{95}}{D_5}. \qquad (12)$$

where D_{95} and D_5 represent the dose received by 95% and 5%, respectively, of the PTV. The closer HI is to its maximum value of 1 the more homogenous the plan is.

Normal lung tissue metrics included the MLD, NTD, V20, V13, and V5 as defined in the first section, as well as the heart, spinal cord and esophagus maximum point dose as defined by RTOG clinical trials[124] (Table VIII).

Table. VIII. RTOG dose limits for hypofractionated lung radiation therapy

	Spinal cord (cGy)	Esophagus (cGy)	Heart (cGy)
Maximum point dose (point dose is defined as a volume of 0.035cc or less)	1800	2520	3000

3.1.4 Statistics

The dosimetric parameters comparison was the primary endpoint for this study and the statistical significance of comparing these parameters is calculated using the non-parametric Wilcoxon signed rank test to account for the small sample size and the pair-matching of parameters between each of the three plans. Differences were reported to be statistically significant at $p \leq 0.05$. Statistical analysis was performed using the Stata Data Analysis Software (StataCorp, College Station, TX).

3.2 Results

PTV metrics

The results showed a general trend where 1-segment and 5-segments plans were more conformal than 3DCRT plans. Both conformality indexes improved significantly ($p=0.0001$ and

p=0.0001): R100 mean for 3DCRT plans was 1.41 compared to 1.17 and 1.15 for 1-segment and 5-segments plans respectively; and CI mean for 3DCRT plans was 0.5333 compared to 0.6866 and 0.7252 for 1-segment and 5-segments plans, respectively. Summary of PTV metrics with p values is shown in Table IX.

Table. IX. Summary of PTV metrics and differences between 1-segment, 5-segments and 3DCRT plans.

		3DCRT	1-segment	5-segment
R100	Mean	1.4100	1.1700	1.1500
	St Dev	0.2545	0.1658	0.1431
	median(min-max)	1.35(1.05-1.90)	1.12(1.00-1.69)	1.10(1.00-1.50)
CI	Mean	0.5333	0.6866	0.7252
	St Dev	0.1546	0.0895	0.0917
	median(min-max)	0.53(0.35-0.90)	0.68(0.49-0.85)	0.72(0.58-0.90)
R50	Mean	5.7150	5.4854	5.5060
	St Dev	1.3488	1.1590	1.1611
	median(min-max)	5.23(2.81-8.2)	5.43(2.75-7.55)	5.54(2.49-7.51)
HI	Mean	0.8178	0.7609	0.7862
	St Dev	0.0641	0.0714	0.0733
	median(min-max)	0.82(0.66-0.92)	0.77(0.57-0.87)	0.81(0.57-0.91)
#MU/PTV	Mean	2066.1200	2104.0000	2216.6400
	St Dev	698.9070	727.0190	725.6400
	median(min-max)	2074.75(375-3344.5)	2021(394.5-3374)	2302(401.25-3401)

	p values		
	3DCRT vs 1-segment	3DCRT vs 5-segment	5-segment vs 1-segment
R100	0.0001	0.0001	0.1863
CI	0.0001	0.0001	0.0013
R50	0.0837	0.225	0.5561
HI	0.0001	0.0458	0.0021
#MU/PTV	0.0783	0.0309	0.0022

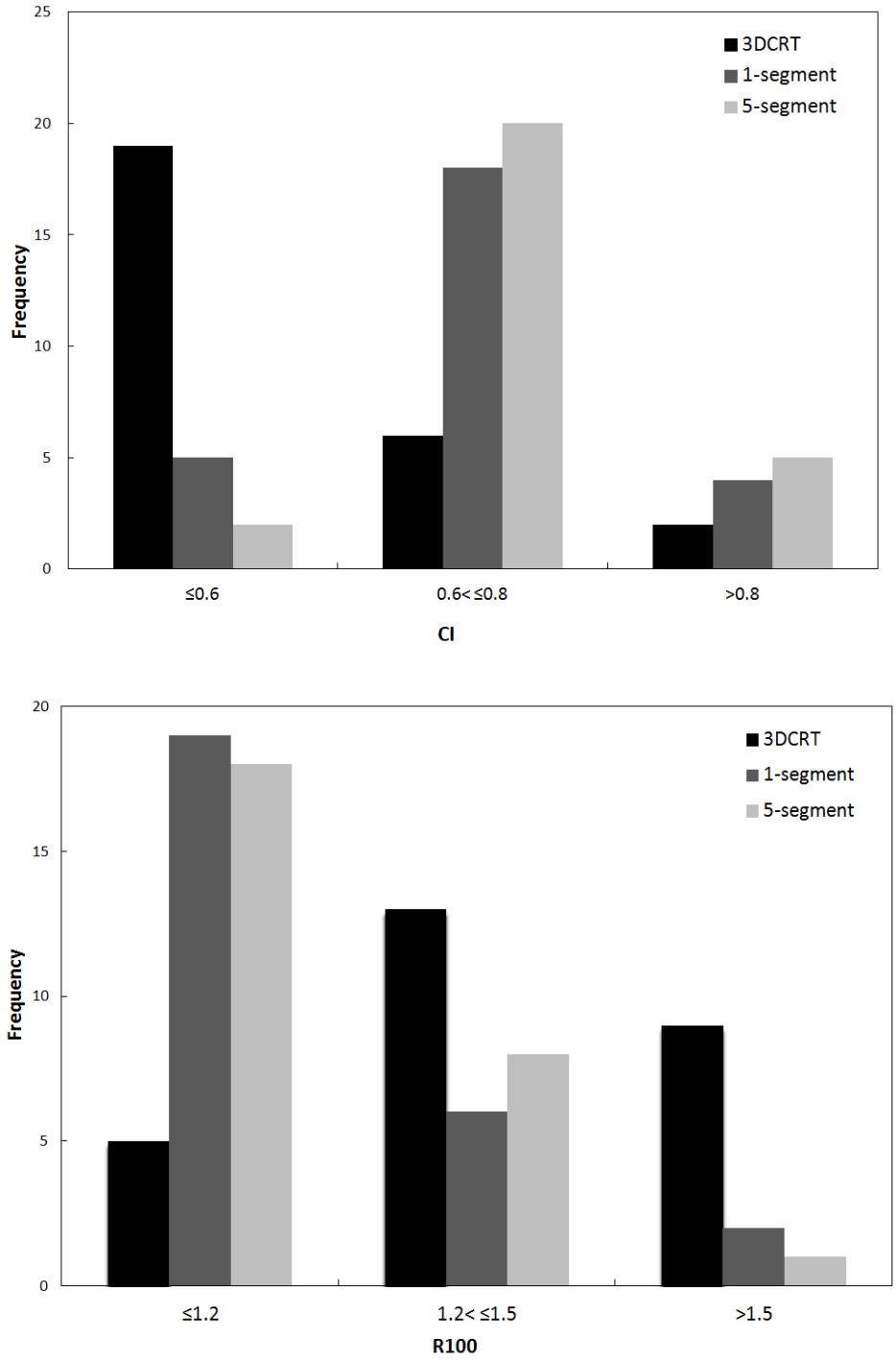

Fig. 10. Bar graph distribution of CI (top) and R100 (bottom)

There was no statistical difference in R100 between 1-segment and 5-segments plans ($p=0.1863$); however CI was significantly improved for 5-segments plans with a mean CI of 0.7252 compared to an mean CI of 0.6866 for 1-segment plans ($p=0.0013$). Figure 10 shows bar graph distributions of R100 and CI. The overall distribution shows consistently superior conformality for 1 and 5-segments plans over 3DCRT plans.

Regarding the dose fall-off at the 50% isodose level, although the mean R50 was lower for 1-segment and 5-segments plans, the p value was >0.05 for both subgroups compared to 3DCRT plans. The dose fall-off at the 50% isodose level showed no statistical differences in R50 between 1-segment and 5-segments plans ($p=0.5561$).

The PTV inhomogeneity also demonstrated a general trend with 1-segment and 5-segments plans being more inhomogeneous than 3DCRT plans. HI was significantly higher for 3DCRT plans compared to both 1-segment and 5-segments plans ($p=0.0001$ and $p=0.0458$). The results showed a general trend where single segment plans were significantly more inhomogeneous than 5-segments plans, with a mean HI of 0.7609 for 1-segment plans and 0.7862 for 5-segments plans ($p=0.0021$). Figure 11 shows the HI values for all the different PTV volumes, and except for the larger PTV, the 1-segment plans were consistently more inhomogeneous than 3DCRT and 5-segments plans.

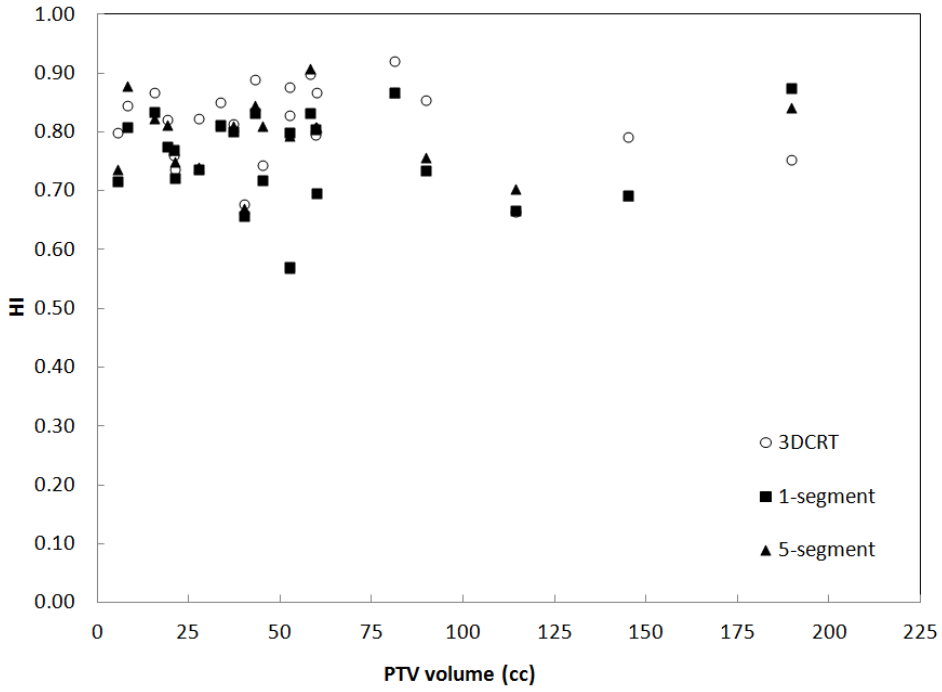

Fig. 11. HI distribution depending on PTV volumes.

On average, the 1-segment plans required 2104 MUs to deliver one fraction of the treatment, compared with 2066 MUs needed on average to deliver one fraction of 3DCRT plan. There was no statistical difference between subgroups (p=0.0783), while it required on average more MUs, 2216, to deliver 5-segments plans compared to 3DCRT plans. The difference in the total number of MUs needed per fraction per PTV between 5-segments and 3DCRT plans was statistically significant (p=0.0309). The other general trend revealed that 5-segments plans needed significantly more MUs per PTV compared to 1-segment plans (p=0.0022).

Since both 1-segment and 5-segments plans had significantly improved conformality compared to 3DCRT plan, we wanted to quantify which technique had the most important improvement. Figure 12 shows the percentage difference for R100 and CI, for both subgroups 1-segment and 5-segments plans relative to 3DCRT plans. The improvement of the 5-segments plans compared to 1-segment plans relative to the 3DCRT plans was significantly better for both conformality indexes R100 and CI (p=0.0001, and p=0.0014, Table X). The improvement of R100 and CI for both subgroups 1 and 5-segments over 3DCRT plans are shown in Fig. 12.

Table. X. Percentage difference of the 1 and 5-segments plans relative to the 3DCRT plans for R100 and CI

		1-segment	5-segment
Percentage difference relative to 3DCRT plans			
R100	Mean	1.1436	16.9772
	St Dev	5.6973	12.1724
	median(min-max)	0.7595(-12.9620-13.7566)	12.88(0.5322-42.1621)
CI	Mean	30.0769	38.7167
	St Dev	21.9056	26.5385
	median(min-max)	27.7422(-14.1414-75.9000)	34.6356(0-99.9893)

Percentage difference relative to 3DCRT plans	p values, 1-segment vs 5-segment
R100	0.0001
CI	0.0014

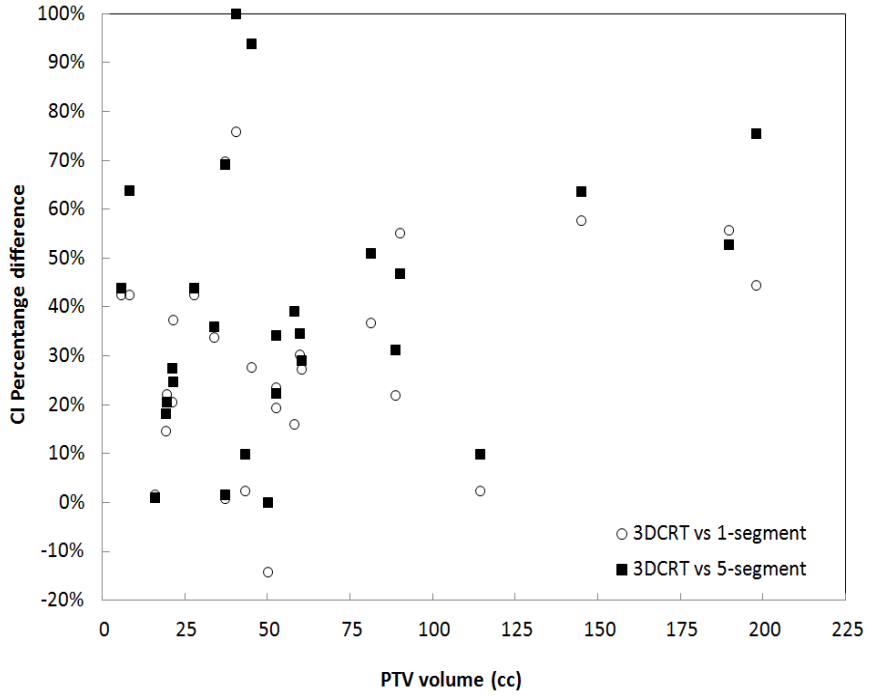

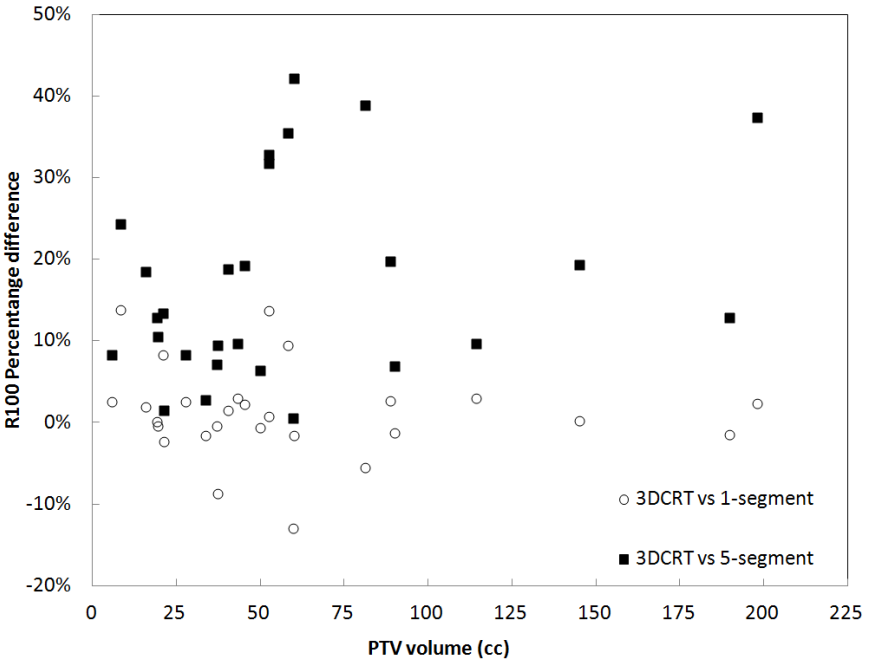

Fig. 12. Percentage difference for R100 and CI, for 1-segment and 5-segments plans and relative to 3DCRT plans.

Organs at risk metrics

The spinal cord, the esophagus and the heart showed no statistically significant differences between 1-segment, 5-segments and 3DCRT plans, with all p values above 0.05 (Table XI). Figure 13 shows the spinal cord, esophagus and heart maximum point dose for each patient.

Table. XI. Summary of maximum point dose for the spinal cord, esophagus and heart for all of the three planning techniques, 3DCRT, 1-segment and 5-segments plans.

Maximum point dose (cGy)		3DCRT	1-segment	5-segment
Spinal cord	Mean	1365.6000	1380.8000	1349.0667
	St Dev	414.7899	388.6681	386.8895
	median(min-max)	1492(497-1798)	1477(448-1778)	1344(513-1778)
Esophagus	Mean	1893.8667	1786.2000	1771.1333
	St Dev	610.9273	630.5654	642.0704
	median(min-max)	1938(497-2510)	2000(584-2510)	1905(485-2508)
Heart	Mean	2220.2000	2288.9333	2253.8667
	St Dev	918.1345	924.1600	935.9479
	median(min-max)	2480(66-2925)	2737(34-2957)	2689(37-2989)

	p values		
Maximum point dose (cGy)	3DCRT vs 1-segment	3DCRT vs 5-segment	5-segment vs 1-segment
Spinal cord	0.8647	0.8203	0.8646
Esophagus	0.2112	0.0509	0.2805
Heart	0.2558	0.5701	0.3201

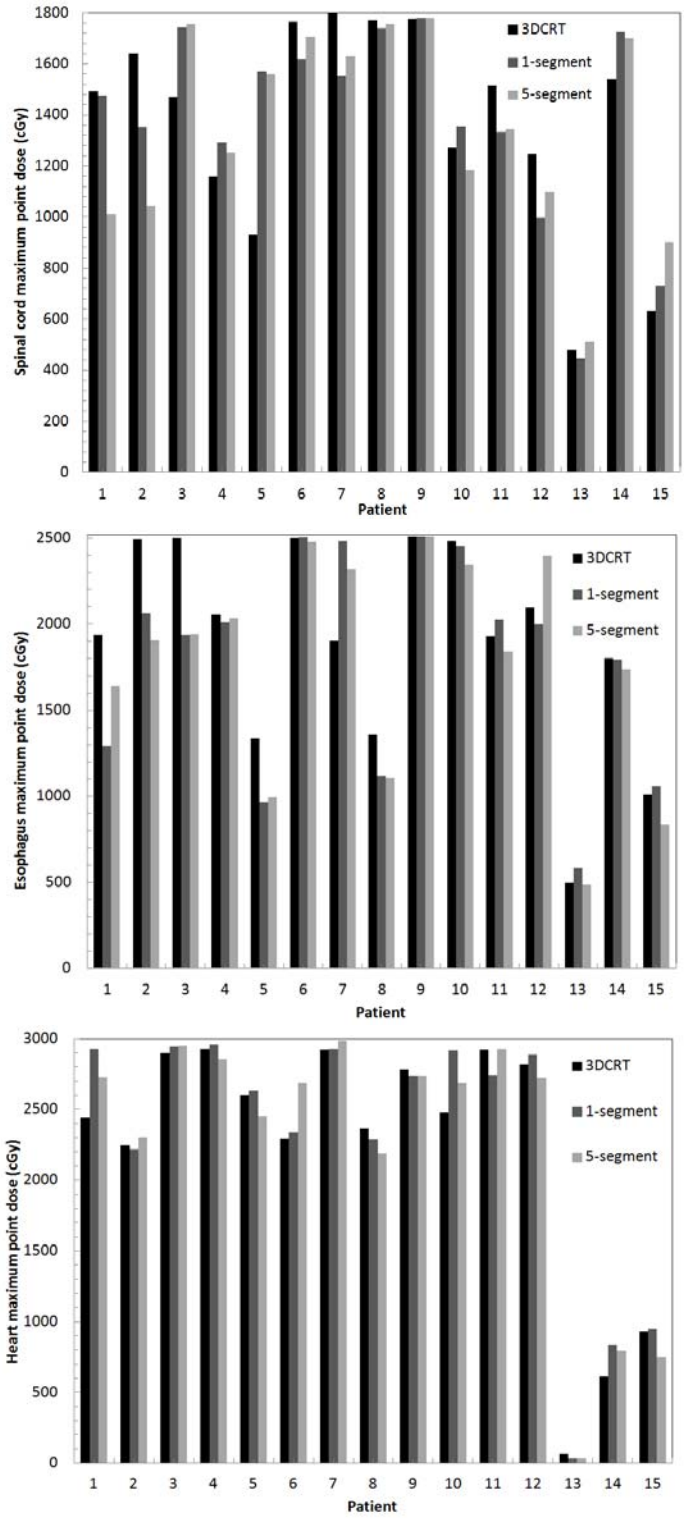

Fig. 13. Spinal cord, esophagus and heart maximum point dose for each patient

Regarding the normal lung metrics, the results showed a general trend where the lung metrics for 1-segment and 5-segments plans were consistently lower than the 3DCRT plans, with p values < 0.05. The V5 mean for 3DCRT plans was 41.0% compared to 37.12% and 37.25% for 1-segment (p=0.0054) and 5-segments (p=0.0106) plans, respectively; the V13 mean for 3DCRT plans was 22.19% compared to 16.01% and 15.77% for 1-segment (p=0.002) and 5-segments (p=0.0031) plans, respectively; the V20 mean for 3DCRT plans was 10.08% compared to 7.97% and 7.89% for 1-segment (p=0.0007) and 5-segments (p=0.0018) plans, respectively; MLD mean for 3DCRT plans was 744.3cGy compared to 658.2 cGy and 653.6 cGy for 1-segment (p=0.0007) and 5-segments (p=0.0007) plans, respectively; and NTD mean for 3DCRT plans was 1275.6 cGy compared to 1128.61 cGy and 1113.39 cGy for 1-segment (p=0.0007) and 5-segments (p=0.0007) plans, respectively. There were no statistical differences for any lung metrics between 1-segment and 5-segments plans, with all of the p values > 0.05. Summary of lung metrics with p values is shown in Table XII. We also computed the NTCP for each patient, and we could observe a consistent reduction in the risk of normal lung tissue complication as shown in the Fig. 14.

Table. XII. Summary of lung metrics (top), p values comparison for all the lung metrics between each of the three planning techniques, 3DCRT, 1-segment and 5-segments plans

Whole lung minus GTV		3DCRT	1-segment	5-segment
V5 (%)	Mean	41.0053	37.1207	37.2553
	St Dev	22.4720	20.2309	20.2250
	median(min-max)	32.50(6.8-82.10)	31.51(7.00-76.30)	30.39(7.00-74.20)
V13 (%)	Mean	22.1907	16.0173	15.7760
	St Dev	21.2230	8.9448	8.6924
	median(min-max)	18.90(2.2-34.90)	15.10(1.20-31.00)	18.72(2.10-31.00)
V20 (%)	Mean	10.0860	7.9720	7.8960
	St Dev	6.1264	4.4353	4.5274
	median(min-max)	10.59(1.20-24.30)	7.74(1.0-15.96)	7.77(1.00-17.34)
MLD (cGy)	Mean	744.3333	658.2000	653.6000
	St Dev	385.3380	311.2340	308.6544
	median(min-max)	641(190-1620)	598(163-1180)	606(164-1166)
NTD(2Gy) (cGy)	Mean	1275.6600	1128.6100	1113.3933
	St Dev	605.8857	534.5731	532.3597
	median(min-max)	1335(245-2264)	1128(214-2264)	1102(271.40-1972.00)

Whole lung minus GTV	*p* values		
	3DCRT vs 1-segment	3DCRT vs 5-segment	5-segment vs 1-segment
V5 (%)	0.0054	0.0106	0.7119
V13 (%)	0.002	0.0031	0.4776
V20 (%)	0.0007	0.0018	0.7542
MLD (cGy)	0.0007	0.0007	0.4774
NTD(2Gy) (cGy)	0.0007	0.0007	0.3785

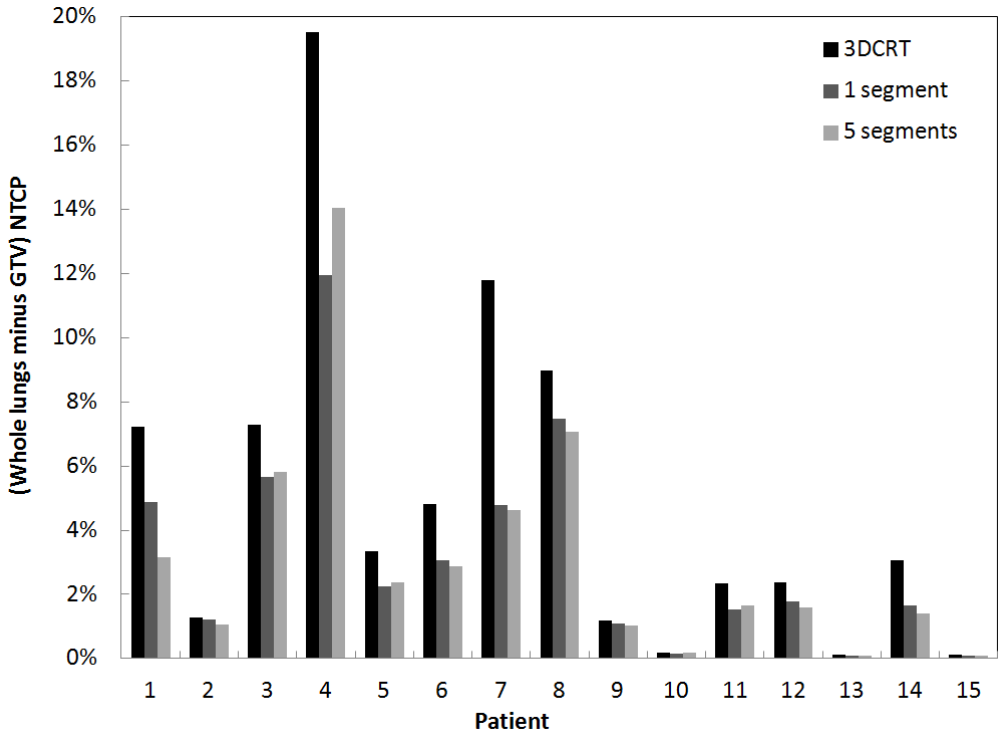

Fig. 14. Normal lung tissue complication probability for each patient and each of the three planning techniques, 3DCRT, 1-segment and 5-segments plans.

Case study: analysis of Case #1

Isodose curves for Case #1 with 4 lesions are presented in Fig. 15, showing 3DCRT, 1-segment and 5-segments plans. This patient received 36 Gy in 3 fractions to RLL, RUL and LUL lesions as well as 30 Gy in 3 fractions to a RML lesion. The total volume of the PTVs receiving 36 Gy was 58.16 cm^3 and the volume of the PTV receiving 30 Gy was 8.22 cm^3. For the PTV receiving 36 Gy, the prescription isodose line in the 1-segment and 5-segments plans was highly conformal to the PTV with a R100 of 1.17 and 1.02, respectively compared to 1.58 for the 3DCRT plan. Similarly, the CI was 0.65 and 0.78 for the 1-segment and 5-segments plans, respectively, compared to 0.56 for the 3DCRT plan. The 50% isodose line volume of the 1-segment and 5-segments plans was reduced with an R50 of 6.97 and 6.05 for the 1-segment and 5-segments plans, respectively, compared to 8.2 for the 3DCRT plan. Similarly, for the PTV receiving 30 Gy, the prescription isodose line in the 1-segment and 5-segments plans was highly conformal to the PTV with a R100 of 1.69 and 1.43, respectively, compared to 1.89 for the 3DCRT plan; the CI was 0.670 and 0.770 for the 1-segment and 5-segments plans, respectively, compared to 0.470 for the 3DCRT plan. For that PTV the R50 of the 3DCRT plan, 4.236, was actually lower than the R50 of the 1-segment and 5-segments plans, 4.85 and 4.789, respectively.

As shown in Fig. 12, the higher isodose lines such as the 105% isodose line was totally enclosed inside the PTV volume for the 1-segment and 5-segments plans. Moreover, the 105% isodose line volume enclosed in the PTVs was more important for the 1-segment plan compared to 3DCRT and 5-segments plans. This could also be observed with the inhomogeneity index, with an HI of 0.90 and 0.91 for the 3DCRT and 5-segments plans respectively, compared to 0.83 for the 1-segment plan for the PTV 36 Gy. Similarly the HI was 0.84 and 0.88 for the 3DCRT and 5-segments plans, respectively, compared to 0.81 for the 1-segment plan for the PTV 30 Gy.

The DVHs for the whole lung minus GTV is shown in Fig. 16 and we observed a net reduction in the dose received by the normal lung tissue, with NTD of 1713.90 cGy for the 3DCRT plan, and reduced to 1534.60 cGy and 1348.80 cGy for the 1-segment and 5-segments plans, respectively, with complication risk of 7.21% for the 3DCRT plan, and reduced to 4.88 % and 3.14 % for the 1-segment and 5-segments plans, respectively.

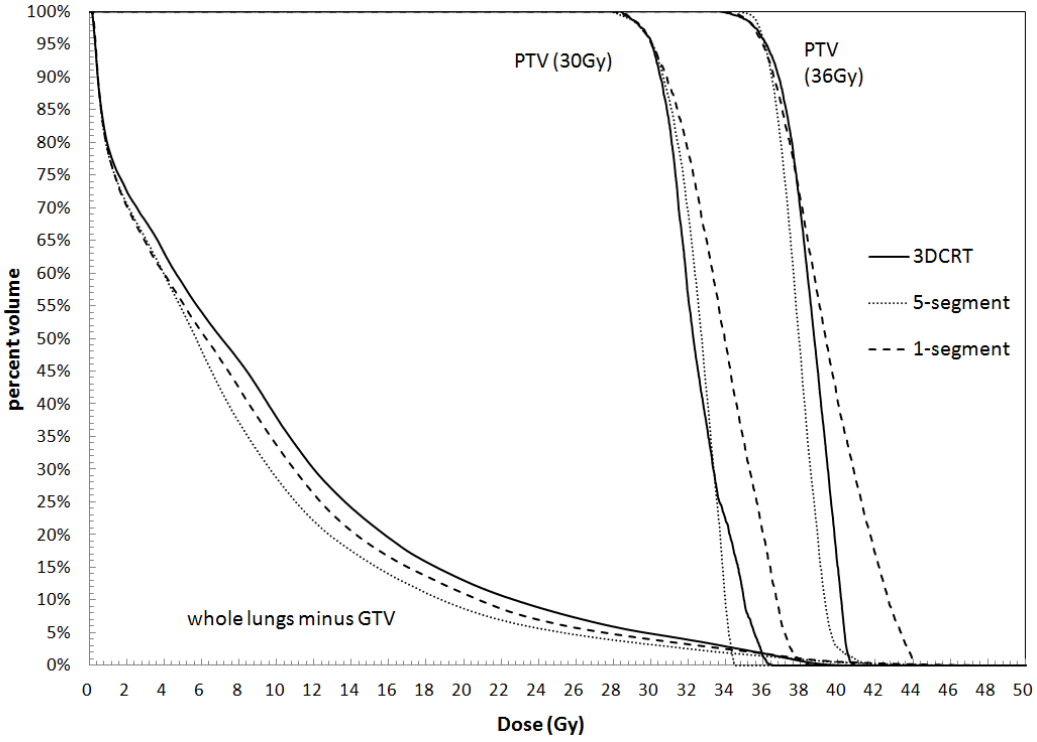

Fig. 15. DVHs for PTVs receiving 30 and 36 Gy and for the whole lung minus GTV for Case #1

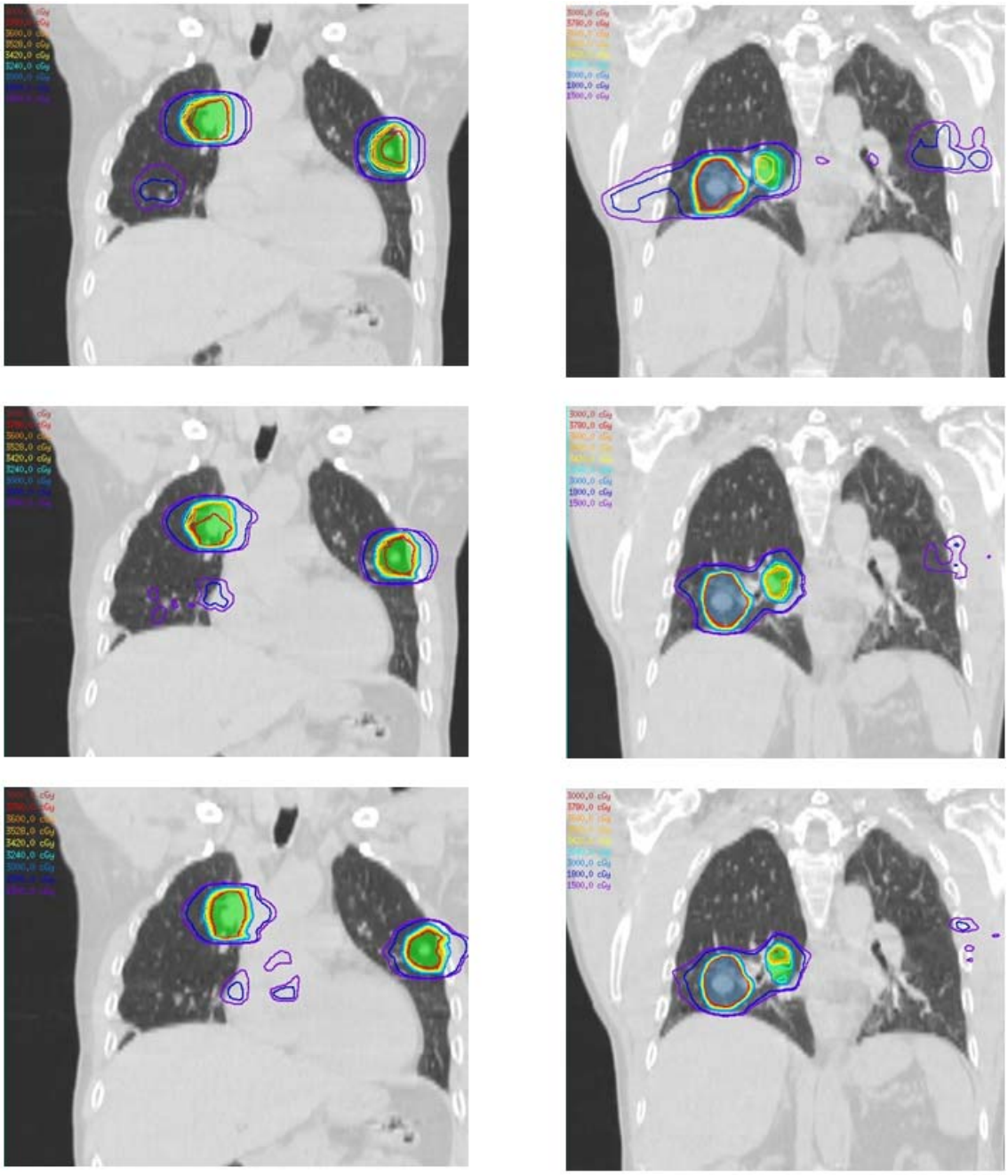

Fig. 16 Isodose curves for Case #1, showing 3DCRT (top), 1-segment (middle) and 5-segments (bottom) plans for all four lesions

3.3 Discussion

To date there has been no retrospective planning study looking at the DMPO algorithm used for lung oligometastasis hypofractioned treatments. This study evaluated the potential effect of a DMPO algorithm, compared with 3DCRT via a retrospective dosimetric analysis. The DMPO algorithm was used with the intent of reducing the complexity of optimized plans to create two plans allowing successively one and five segments per beam.

Fifteen lung HIGRT cases were selected, all of them having at least 2 oligometastasis lesions. The reasons for choosing this type of cases in this study were twofold. First, in the context of HIGRT the planning process is often complex and cumbersome; it was attractive to see if an inverse planning algorithm could be used to automate the process while trying the keep the plan complexity as low as possible with a minimum amount of segments. Second, radiation therapy for multiple targets in the lungs constituted a challenge for the planner to cover the target with the prescription isodose line while sparing the normal surrounding tissue. We purposely selected the most challenging cases with multiple PTVs; cases for which 3DCRT might reach its limitations in terms of PTV conformality and normal tissue sparing, and for which inverse optimization with DMPO might be a solution.

Therefore, the main focus of this study was to establish the potential benefits of 1-segment and 5-segments DMPO techniques, in keeping normal organ at risks below dose tolerance, in reducing normal lung dose, and in improving target coverage and conformality.

There was a significant improvement of the CI and R100 with the 1-segment and 5-segments plans compared to 3DCRT plans (Table V and Fig. 9). Even though there was no significant difference in R100 between 1- and 5-segments plans, the CI showed significant improvement for 5-segments plans over 1-segment plans. The improved conformality can be explained by the increased complexity of the 5-segments plans since more segments allow for

better dose painting around the PTV. A Japanese study[125] reported that less conformal plan could be associated with higher risk of radiation pneumonitis, therefore using 5-segments plans could be preferable in our context of multiple lung metastases. However the deliverability to a moving target of multiple segment plans needs to be addressed and will be discussed in the next section. In addition we observed that 5-segments plans requires significantly more MUs than 3DCRT and 1-segment plans, which could result in an increase in secondary malignancies[126] . Therefore, the benefit of the improved conformality with 5-segments plans is counterbalanced by an increase in plan complexity and number of MUs.

Also we showed that 1-segment plans deliver highly inhomogeneous dose inside the PTV. The inhomogeneity metric, HI, was significantly lower with 1-segment plans compared to 3DCRT and 5-segments plans. The HI value indicated that the amount of dose higher than the prescription dose such 105% and 110%, was significantly more important for 1-segment plans. We considered this increase in dose inside the tumor clinically acceptable and even beneficial for two reasons; first it resulted in a higher BED inside the tumor hence increasing the tumor control probability, second it could help by targeting more efficiently the radio-resistant hypoxic cells inside the tumor. High levels of hypoxia in tumors have been associated with treatment failures in radiation therapy[127]. While fractionated radiation therapy over three to four weeks allows for reoxygenation between fractions[128], hence reducing the influence of hypoxic cells, this is not true with HRT with a course of only 3 fractions. Therefore we could advocate that highly inhomogeneous plans like 1-segment plans could circumvent the hypoxia-induced radio-resistance and be more beneficial than 5-segments or 3DCRT techniques.

We believe that the most significant finding in the present study was that, in addition to improving the PTV conformality, DMPO optimization allowed us to significantly reduce the MLD as well as the NTD, V20 and V13 for the normal lung tissue. In the previous section of this

project, we showed that all these parameters, MLD, NTD, V20 and V13 were statistically significant predictors for RP Grade ≥ 2. Therefore the results obtained with 1-segment and 5-segments plans could be very helpful in reducing the risk of RP. There were no statistical differences in any of the lung metrics between 1- and 5-segments plans; hence we would once again support the use of 1-segment over 5-segments plans. The plans with 1-segment per beam were simplified and could also reduce the overall treatment time delivery, which could also be of great benefit in our patient cohort with multiple lung metastases.

In addition to the possibility of sparing the lung with the use of DMPO plans we were able to keep the spinal cord, esophagus and heart maximal dose within tolerance. In some cases, we were even able to substantially reduce to esophagus and heart maximal dose by incorporating it as constraints in the optimization. Since acute esophagitis and long-term cardiac toxicity can be significant limiting factors in the treatment of lung lesions, dose reduction to these structures should benefit from DMPO plans.

However, the improved conformality should be viewed cautiously since it increases the risk of a geometric miss if the setup error is bigger than the setup uncertainty added to the ITV or if the internal target motions are not accounted for correctly. High-dose-gradient increases the risk of underdosing the tumor and overdosing the surrounding normal tissue. One of the main impediments in HIGRT delivery is the precision of dose actually delivered at treatment relative to the dose planned. Set-up errors are reduced by the use of imaging-guidance tools described above, and internal target motions are accounted for via a 4D-CT and the method described above. To increase the level of accuracy of tumor definition and localization, functional imaging, such as fluorodeoxyglucose positron emission tomography can help address the challenge of tumor delineation [129-130]. A rigid respiratory phantom has been used to verify and validate the DMPO techniques for lung HIGRT.

3.4 Conclusion

The “forward planning step”, the first step consisting of choosing collimator angle and non-coplanar beam angle, minimizes the normal lung exposure to radiation. The “inverse planning step”, the second step consisting of using the DMPO algorithm to optimize beam apertures and weights, maximizes PTV coverage and minimizes normal tissue doses. Using this method we do not have any additional degrees of freedom compared to traditional 3DCRT, but rather use the optimization routine for our benefit.

Standard forward 3DCRT planning techniques could be improved by incorporating an inverse planning approach. Single segment plans were able to significantly improve tumor coverage and conformality, reduce the risk of lung RP, while simplifying the planning process and delivery. Target conformality and normal lung tissue sparing did not gain much improvement from an increase of plan complexity to five segments over the simplified one segment technique.

The automation of our method is a good alternative to more traditional methods and offers significant dosimetric benefits.

Despite the benefits of the DMPO 1-segment techniques, a rigorous and careful validation via phantom measurement is necessary and will be presented in the following section.

4. AIM 3: VERIFY AND VALIDATE THE PLANNING TECHNIQUE PRESENTED IN AIM 2 VIA DOSIMETRIC QA DELIVERED ON A MOTION PHANTOM

4.1 Materials and methods

One of the main impediments in HRT delivery is the precision of dose actually delivered at treatment relative to the planned dose. As mentioned above tight margins and precise dose shaping are among the hallmarks of HRT. Dose delivery accuracy in HRT needs to be addressed even more so when targets are in the lung and delivery imprecision due to respiratory motion might occur. The AAPM Task Group Report 101[40] on SBRT suggests the use of a respiratory phantom to perform end-to-end testing and verification of the SBRT process. Besides, IMRT requires patient-specific QA involving a dosimetric verification comparing the planned dose with the delivered dose [131] [132]. As our approach developing plans with one segment per beam angle involved both inverse planning as well as hypofractionated dose regimen, we report in this section on patient-specific quality assurance for the 1-segment planning technique developed in the previous section.

A rigid phantom (QUASAR respiratory Motion Phantom, Modus medical Devices Inc., London, Canada) was used to simulate one-dimensional, respiratory-induced movement. A motor moves a platform on which is placed an infra-red reflecting block from the RPM system, as well as a cylindrical lung insert, so that they both move with the same period (Fig. 17). Amplitude and period of the sinusoidal motion for the platform and the lung insert can be adjusted.

A special lung-equivalent insert (Fig. 18), was manufactured from cork material. The total cork cylinder was 18 cm long with a 7.70 cm diameter. A tissue-equivalent polyethylene cylinder 3 cm long and 1.90 cm in diameter was located in the geometrical center of the cork

cylinder, simulating a tumor in lung (Fig. 19). A 4DCT scan of the phantom was acquired for the respiratory phantom and the tissue-equivalent target was contoured and defined as the ITV. We added 5 mm in all directions to the ITV to generate the PTV.

Fig. 17. QUASAR respiratory motion used for patient-specific QA

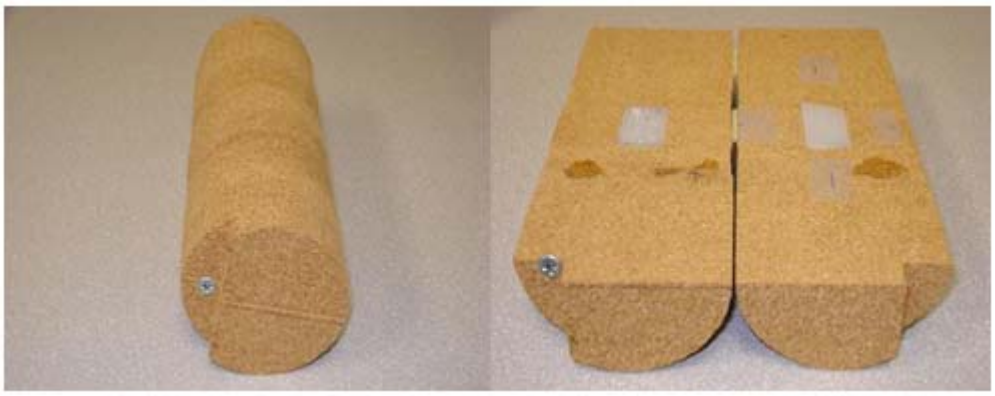

Fig. 18. Lung insert with tissue equivalent target used to simulate a target in lungs in the respiratory phantom.

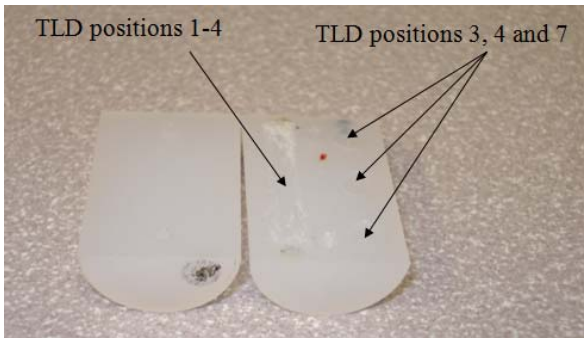

Fig. 19. Tissue equivalent target used to simulate a tumor is lung with TLD positions

Film measurements

The lung insert was designed in such a way that radiochromic films, Gafchromic EBT2 (ISP Corp., Wayne, NJ, USA) could be fitted between the sections of this phantom. Radiochromic films have been reported to offer high resolution, planar dose measurement with reduced energy dependence, ideal for measurements of high gradient radiation fields[133]. Radiochromic films consist of a double layer of radiation-sensitive organic microcrystals on a thin polyester base with a transparent coating. The film is darkened by radiation, and the darkness increases with increased absorbed dose. Radiochromic films do not require processing to develop the image. Once the film is read using a flat bed scanner, isodose curves are created and converted into dose with a calibration curve acquired before the phantom irradiation.

To evaluate the difference between calculation and film measurement, we looked at the dose to distance agreement criteria of 3%/3 mm developed by Low *et al.*[134], as well as the tighter dose to distance agreement criteria of 2%/2 mm. Figure 20 shows a representation of the method for 2D dose distribution verification and looking simultaneously at distance to agreement and dose difference. The gamma is defined as:

$$\Gamma(r_m, r_c) = \sqrt{\frac{r^2(r_m, r_c)}{\Delta d_M^2} + \frac{\delta^2(r_m, r_c)}{\Delta D_M^2}}, \quad (13)$$

where $r(r_m, r_c) = |r_c - r_n|$ and $\delta(r_m, r_c) = D_c(r_c) - D_m(r_m)$

Δd_M represent the distance to agreement passing criteria, 3 and 2 mm in our study

and ΔD_M represent the dose difference passing criteria, 3 and 2%.

$$\gamma = \min\{\Gamma(r_m, r_c)\} \forall \{r_c\}, \quad (14)$$

if $\gamma \leq 1$, calculation passes,

if $\gamma > 1$, calculation fails.

Radiochromic films were inserted along the coronal plane and irradiated with optimized segment beams to evaluate the dose in the lung and in the target. The gamma analyses were performed using the FilmQA software (3cognition, Wayne, NJ)

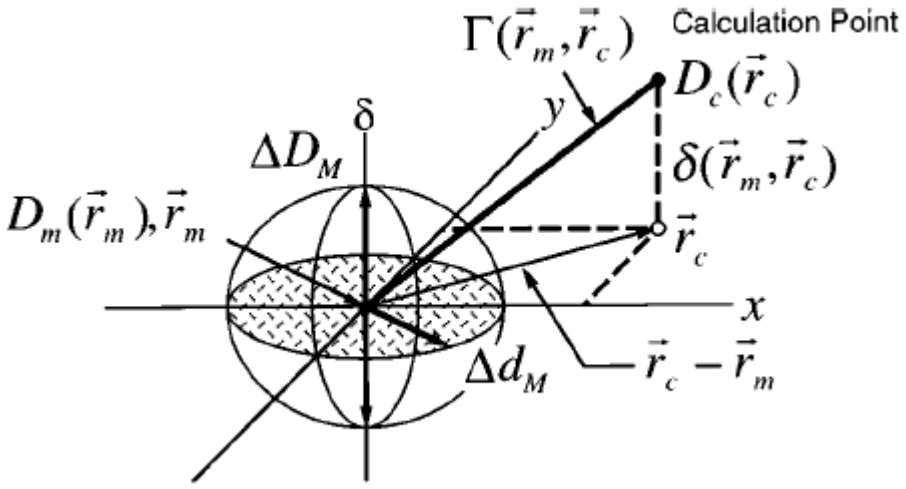

Fig. 20. Geometric representation of dose distribution evaluation criteria using the combined dose difference and dose to agreement criteria defined by Low *et al.*[134].

TLD measurements

The use of TLDs in radiation therapy for *in vivo* dosimetry has been described [135] [136]. To also perform absolute dose verification, we inserted in the tissue equivalent target TLD at seven locations throughout the target (Fig. 19) and compared the measured doses with the planned doses. We used lithium fluoride TLDs in this study.

Before each phantom irradiation, the TLDs were annealed for 1 h at 400 °C , and 18 h at 80 °C. We evaluated the individual TLD sensitivities by exposing them to a 6 MV beam with known dose at a depth of 10 cm, with a 10 cm × 10 cm field size, and at a source to axis distance (SAD) of 100 cm. We performed three sensitivity exposures for all the TLDs used in this study. We compared the reading of each TLD to the average reading and calculated the sensitivity and its standard deviations for each TLD. Finally, we averaged the three sensitivities to estimate the sensitivity used for dose measurements. After each phantom irradiation we also performed TLD dose calibration, by exposing the TLDs to a known dose, and derived the calibration factors used to convert charge readings to dose.

However, we measured absorbed dose in a tissue-equivalent target of polyethylene, while the dose calculated by the treatment planning system was absorbed dose in water. We therefore corrected each reading via the Burlin cavity theory[137] using the mean ratio of mass collision stopping power of polyethylene and water as well as the mean ratio of the mass energy absorption coefficient of polyethylene and water.

4.2 Results

The volume of the target used in this study was 8.5 cm^3 and we selected PTVs among the multiple metastases cohort with comparable target sizes, Case #1, #10 and #11, with PTV volumes of 8.22 cm^3, 5.7 cm^3 and 8.6 cm^3 respectively. We performed patient-specific QA on

each of the case according the method described previously. We copied the treatment beams and projected them onto the respiratory phantom geometry as shown in Fig. 21. Figure 22 shows the optimized MLC apertures for the LUL target of Case #11 receiving a total dose of 48 Gy in three fractions. Nine beam angles were used for that plan.

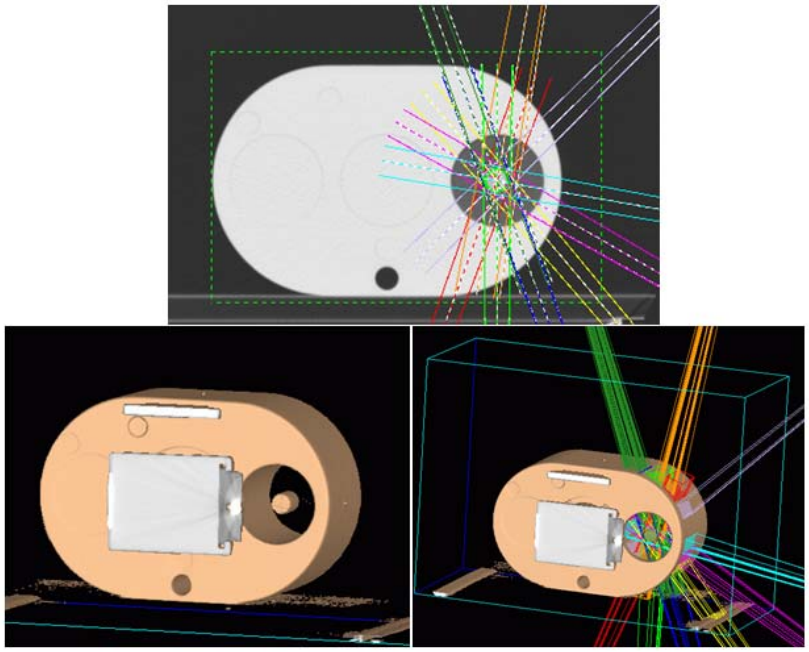

Fig. 21. Axial view of the phantom with treatment beams applied from Case #11 (top), 3D view of the phantom with treatment beams (bottom)

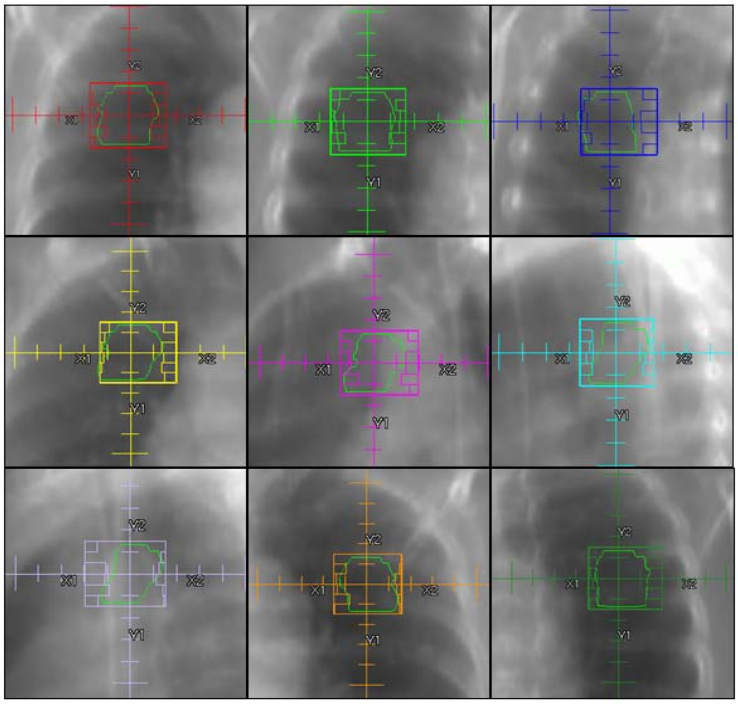

Fig. 22. Optimized MLC apertures for patient #11

Figure 23 shows the isodose regions for LUL targets for Case #11 computed on the respiratory phantom scan. Table XIII shows the measured dose at various locations throughout the target and relative to the measured dose. There were no noticeable differences between the planned and measured doses inside the targets for all three patients. All locations inside the target showed good agreement of the measured dose relative to the planned dose, varying from 102.35±2.3% to 97.98±2.3%.

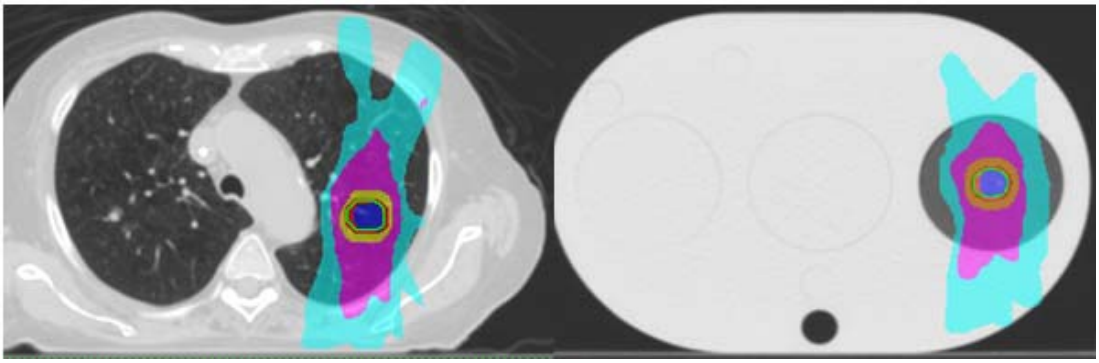

Fig. 23. (Left) Isodose curves for LUL target treated for patient #11 with nine beams (25%, in blue, 50% in pink, 80% in orange, 100% in red, and 105% in blue isodose regions are displayed. (Right) The nine beams were applied and computed to the respiratory phantom geometry, and the same isodose regions are displayed.

Table. XIII. Dose at seven locations inside the target measured with TLD for patient #1, 10 and 11. All doses are expressed in percentage relative to the planned dose.

	TLD measured dose in the target relative to the planned dose (%)						
Patient ID#	Position 1	Position 2	Position 3	Position 4	Position 5	Position 6	Position 7
1	102.35 (±2.3)	99.84 (±1.9)	99.58 (±2.3)	98.78 (±2.1)	101.54 (±1.8)	100.54 (±2.4)	100.77 (±2.5)
10	101.35 (±1.7)	98.57 (±1.2)	101.03 (±2.0)	101.05 (±2.1)	100.35 (±2.5)	99.54 (±2.2)	98.88 (±2.4)
11	102.27 (±2.0)	97.98 (±2.1)	101.36 (±2.2)	101.98 (±2.5)	99.89 (±2.1)	99.54 (±2.3)	98.78 (±1.5)

Figure 24 shows on the left, the dose fluence calculated by the treatment planning system for the 1-segment plan aiming at the LUL lesion of Case #11, and on the right it is the scanned images of the films exposed with the same 1-segment plan. Figure 25 shows a good agreement between calculated and measured dose profiles in the target.

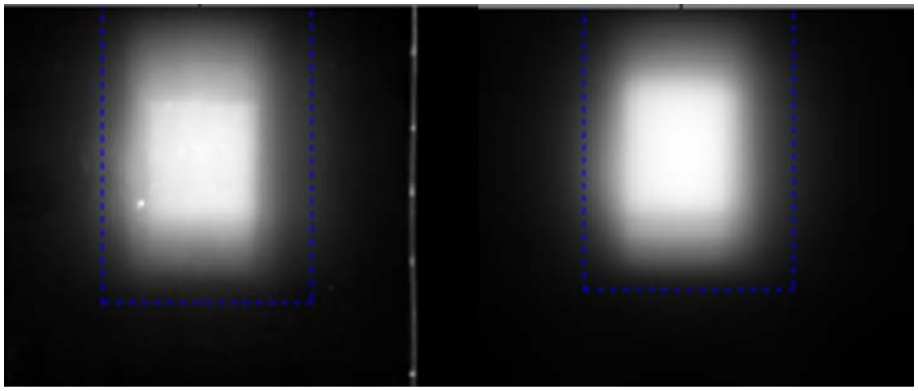

Fig. 24. (left) Dose fluence inside the target computed with the planning system. Images of the scanned Radiochromic films after being exposed with the treatment beams copied from patient #11.

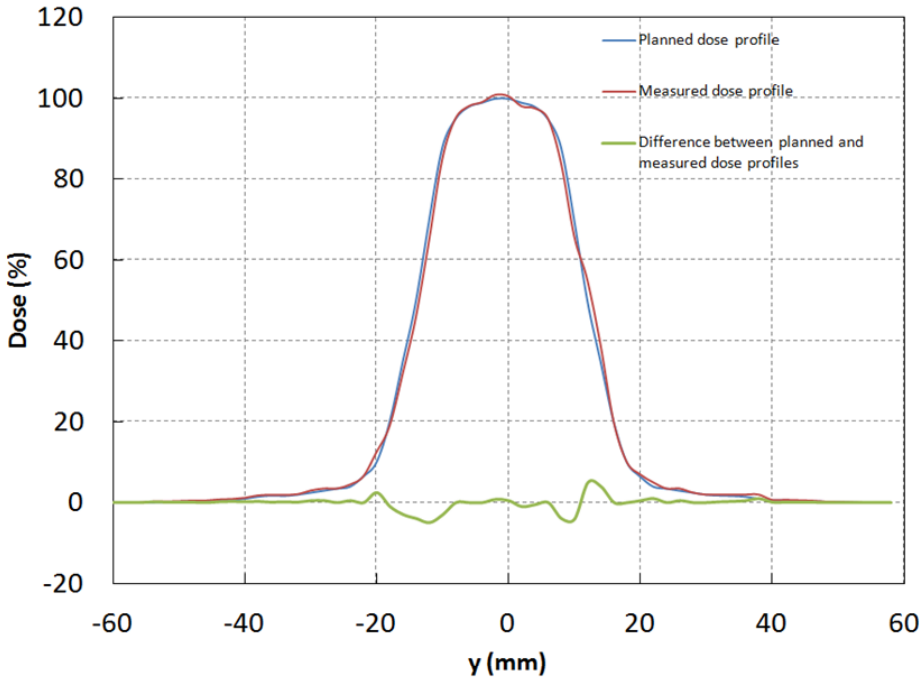

Fig. 25. Dose profiles along the y direction (cranial-caudal), showing the planned dose profile in blue, the measured dose profile in red, and the difference between both profiles in green.

We performed gamma analysis comparing the measured and calculated dose fluence, according to the method described previously. Figure 26 depicts a histogram of the counts sorted by gamma values. There was a good agreement between the exposed film and the calculated fluence, 99.84% of all the measured points had a gamma value less than 1 with the 3%/3mm criteria. Table XIV shows a summary of all the passing rates for Cases #1, 10 and 11. The minimum passing rates were 98.99% for the 3%/3mm criteria, and 97.24% for the tighter 2A%/2mm criteria, which shows good agreement between the measured and calculated dose fluences.

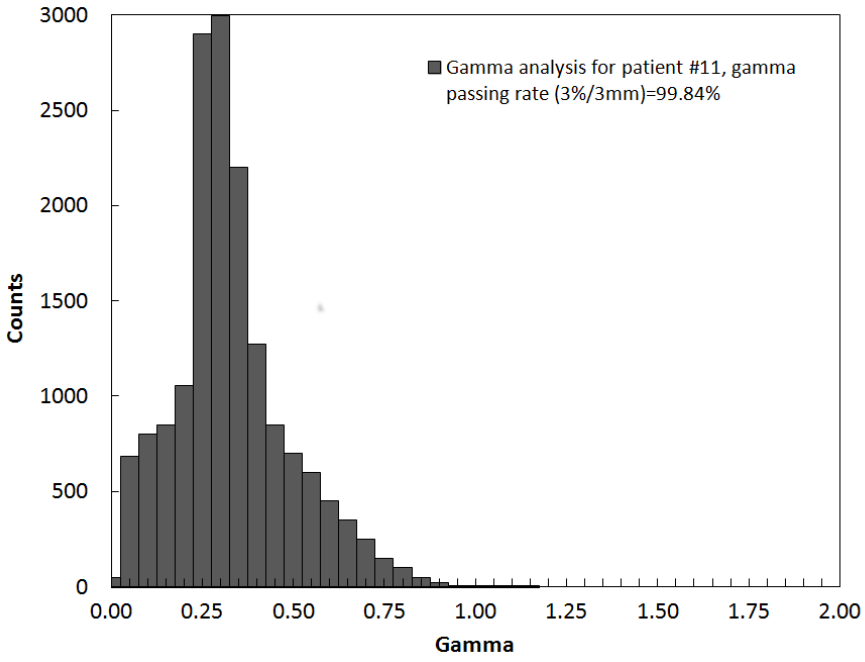

Fig. 26. Histogram of the measured counts sorted by their gamma value. 99.84% of all the counts passed the criteria of 3%/3mm with a gamma values smaller than 1.

Table. XIV. Summary of the passing rates for patients #1, 10 and 11, with both criteria, 3%/3mm as well as 2%/2mm.

	Gamma criteria 3%/3mm			Gamma criteria 2%/2mm		
Patient ID#	All	Tumor	Lung	All	Tumor	Lung
1	99.36	99.05	98.99	98.71	98.02	98.12
10	99.15	99.54	99.12	97.62	98.15	97.36
11	99.84	99.87	99.37	97.98	97.24	97.15

4.3 Discussion

Several authors have studied that the use of IMRT when treating a moving target[57-60] and concluded that the interplay between organ motion and leaves motion is not dosimetrically significant in the case of fractionated radiation therapy delivered over thirty fractions[138]. Clinical outcomes for NSCLC patients treated with IMRT also showed promising results in terms of survival as well as lung and esophagus toxicity [139] [140]. Similarly, investigators published on the use of IMRT in lung HRT; Kang *et al.*[141] evaluated the tumor motion effects on dose distribution for hypofractionated IMRT of NSCLC and concluded that for typical tumor geometries and respiratory amplitudes, changes in target coverage were minimal. Seco *et al.*[142] concluded that for most clinical cases, any non-negligible effects of IMRT dose delivery may be irrelevant with the use of many beams. Videtic *et al.*[49] also showed encouraging clinical outcomes for lung patients treated with hypofractionated IMRT with good local control and survival.

The new planning technique developed in the second part of this study is a simplified IMRT plan with one segment per beam angle. Figure 22 shows an example of optimized MLC

apertures for the LUL target of Case #11. The MLC apertures were derived from the inverse optimization DMPO algorithm as described in the previous section. The PTV contoured is highlighted in green on the DRR. We observe that the shapes of the MLC are mostly surrounding the PTV, with few MLC leafs blocking part of the target, as IMRT segments usually do. Although more simple than multi-segment IMRT plans, these non-intuitive optimized MLC apertures needed to be verified on a phantom.

We showed that a 1-segment technique significantly improved conformality and lung toxicity probability compared to 3DCRT plans and that 1-segment plan significantly use less MUs per PTV compared to 5-segments plans. Even though the 1-segment technique is a very much simplified technique delivery compared to 5-segments technique, we still need to perform a careful validation via phantom measurement. In addition, we showed in the previous section that the 1-segment plans were significantly more inhomogeneous than 3DCRT and 5-segments plans with more important volumes of higher doses confined in the PTV. Therefore, the dose gradient from the center to the edges of the PTV is sharper for 1-segment plans and needs to be verified.

We measured point doses with TLD and compared them with planned doses and found good agreement between planned and measured doses for all three PTV doses we verified. Verifying the dose inside the target was of great importance, especially in the context of the 1-segment plan having higher doses present inside the targets. As mentioned in the previous section, having high dose, such 105% and 110% of the prescription doses inside the PTVs could be critical with hypofractionated dose regimen with only three fractions and where high doses inside the target can help fight hypoxia-induced radio-resistance cells.

The TLD dose measurements inside the target were also important as they served to verify the dose calculation and the dose computation algorithm. In the context of lung radiation

therapy the effect of loss of lateral electron equilibrium has been studied for low and high energy photon beams [143] [144] [145]. Mah *et al.*[146] reported on the impact of tissue inhomogeneity corrections in clinical thoracic radiation therapy and concluded that if lung corrections were not correctly applied the dose within the target could significantly be miscalculated and the radiation-induced normal lung complication probability could be underestimated by at least 5%. The verification of the calculated dose within the target was therefore an important benefit in this study.

Results showed a minimum 98.99 % and 97.24% dose to distance agreement at 3%/3 mm and 2%/2 mm respectively between calculation and films. Although the distance to agreement results at 2%/2 mm were not as good as the distance to agreement results at 3%/3 mm, they were still satisfactory for both criteria. No discernable discrepancies were noted. For each patient we verified the good agreement between calculated dose and the film measurements inside the target and the normal tissue. The confirmation on a respiratory phantom that the calculated dose was correctly delivered was critical for the validation of the 1-segment technique to verify that the improvement in normal lung tissue and tumor metrics could be delivered with high levels of precision and accuracy

4.4 Conclusion

We implemented a QA method via phantom measurement to validate the 1-segment planning technique proposed in this study. We found good agreement between calculated and measured doses. This patient specific QA method provides an integral QA tool for lung hypofractionated radiation therapy and for the 1-segment planning technique.

5. CONCLUSION AND FUTURE WORK

The problem statement of this study was how to improve the implementation of lung HRT. Lung toxicity is one of the main limiting factors in lung HRT, the first aim was to establish possible dose-effect parameters predicting lung RP. We showed that a dose-effect between NTD and RP may exist up to 48 Gy in three fractions as a predictor of lung toxicity.

In the second aim we investigated a new planning method to reduce lung toxicity probability using the predictors identified in the first aim. We developed a planning method which automates the planning process for lung HRT and simplifies its delivery. In this study we used IMRT techniques delivered with a static gantry. To our knowledge no studies have explored before the use of IMRT in lung HRT with a highly simplified delivery down to one segment per beam angle. The results concerning the new planning method were promising; it significantly improved tumor coverage and conformality as well as reduced the risk of lung RP. Further planning analysis could be performed, exploring rotational delivery technique as well as proton radiation therapy. Both of these methods present challenges in the context of lung HRT: rotational therapy introduces gantry rotation as a degree of freedom but also introduces possible interplay motions between gantry rotation and tumor in lungs; and proton therapy takes advantage of the finite range of protons in tissue but tumor motion may be detrimental. Comparison of these techniques with static gantry IMRT techniques used in our study could help determine if one technique is more advantageous than others.

The third aim served as a validation via phantom measurement of the new planning technique developed in the second aim. The patient specific analysis provided a QA tool for the single segment planning technique and we were able to validate the new technique. Furthermore, possible future work could be the use of cancer cell lines implemented in the respiratory phantom and irradiated with hypofractionated lung regimen to investigate the influence of

temporal delivery. Cell survival data from HRT could be used to either derive dedicated parameters for hypofractionated LQ model or determine if other cell survival models could be superior at describing the cell kill with high a dose per fraction.

REFERENCES

[1] L. Leksell, "The stereotaxic method and radiosurgery of the brain," Acta Chir Scand **102**, 316-319 (1951).

[2] A. J. Hamilton, B. A. Lulu, H. Fosmire, B. Stea and J. R. Cassady, "Preliminary clinical experience with linear accelerator-based spinal stereotactic radiosurgery," Neurosurgery **36**, 311-319 (1995).

[3] M. Uematsu, A. Shioda, K. Tahara, T. Fukui, F. Yamamoto, G. Tsumatori, Y. Ozeki, T. Aoki, M. Watanabe and S. Kusano, "Focal, high dose, and fractionated modified stereotactic radiation therapy for lung carcinoma patients: A preliminary experience," Cancer **82**, 1062-1070 (1998).

[4] R. Timmerman, L. Papiez, R. McGarry, L. Likes, C. DesRosiers, S. Frost and M. Williams, "Extracranial stereotactic radioablation: Results of a phase I study in medically inoperable stage I non-small cell lung cancer," Chest **124**, 1946-1955 (2003).

[5] R. Timmerman, L. Papiez and M. Suntharalingam, "Extracranial stereotactic radiation delivery: Expansion of technology beyond the brain," Technol Cancer Res Treat **2**, 153-160 (2003).

[6] L. Papiez, R. Timmerman, C. DesRosiers and M. Randall, "Extracranial stereotactic radioablation: Physical principles," Acta Oncol **42**, 882-894 (2003).

[7] B. D. Kavanagh, R. D. Timmerman, S. H. Benedict, Q. Wu, T. E. Schefter, K. Stuhr, S. McCourt, F. Newman, R. M. Cardinale and L. F. Gaspar, "How should we describe the radioblologic effect of extracranial stereotactic radlosurgery: Equivalent uniform dose or tumor control probability?," Med Phys **30**, 321-324 (2003).

[8] S. B. Curtis, "Mechanistic models," Basic Life Sci **58**, 367-382; discussion 382-366 (1991).

[9] V. Antipas, R. G. Dale and I. P. Coles, "A theoretical investigation into the role of tumour radiosensitivity, clonogen repopulation, tumour shrinkage and radionuclide RBE in permanent brachytherapy implants of 125I and 103Pd," Phys Med Biol **46**, 2557-2569 (2001).

[10] M. Ljungman, "The DNA damage response--repair or despair ?," Environ Mol Mutagen **51**, 879-889 (2010).

[11] R. G. Dale, "The application of the linear-quadratic dose-effect equation to fractionated and protracted radiotherapy," Br J Radiol **58**, 515-528 (1985).

[12] H. D. Thames, "An 'incomplete-repair' model for survival after fractionated and continuous irradiations," Int J Radiat Biol Relat Stud Phys Chem Med **47**, 319-339 (1985).

[13] D. J. Brenner, L. R. Hlatky, P. J. Hahnfeldt, Y. Huang and R. K. Sachs, "The linear-quadratic model and most other common radiobiological models result in similar predictions of time-dose relationships," Radiat Res **150**, 83-91 (1998).

[14] R. K. Sachs and D. J. Brenner, "The mechanistic basis of the linear-quadratic formalism," Med Phys **25**, 2071-2073 (1998).

[15] E. J. Hall, "Repair of radiation damage and the dose rate effect", in *Radiobiology for the Radiologist*, edited by Lippincott Williams & Wilkins (Philadelphia, 2000), pp.67-90.

[16] J. C. Horiot, R. Le Fur, T. N'Guyen, C. Chenal, S. Schraub, S. Alfonsi, G. Gardani, W. Van Den Bogaert, S. Danczak, M. Bolla and et al., "Hyperfractionation versus conventional fractionation in oropharyngeal carcinoma: Final analysis of a randomized trial of the EORTC cooperative group of radiotherapy," Radiother Oncol **25**, 231-241 (1992).

[17] D. J. Brenner, "Hypofractionation for prostate cancer radiotherapy--what are the issues?," Int J Radiat Oncol Biol Phys **57**, 912-914 (2003).

[18] J. V. Lebesque and R. B. Keus, "The simultaneous boost technique: the concept of relative normalized total dose," Radiother Oncol **22**, 45-55 (1991).

[19] M. K. Martel, R. K. Ten Haken, M. B. Hazuka, M. L. Kessler, M. Strawderman, A. T. Turrisi, T. S. Lawrence, B. A. Fraass and A. S. Lichter, "Estimation of tumor control probability model

parameters from 3-D dose distributions of non-small cell lung cancer patients," Lung Cancer **24**, 31-37 (1999).

[20] R. R. Langley and I. J. Fidler, "Tumor cell-organ microenvironment interactions in the pathogenesis of cancer metastasis," Endocr Rev **28**, 297-321 (2007).

[21] S. Paget, "The distribution of secondary growths in cancer of the breast. 1889," Cancer Metastasis Rev **8**, 98-101 (1989).

[22] U. Pastorino, "Lung metastasectomy: why, when, how," Crit Rev Oncol Hematol **26**, 137-145 (1997).

[23] S. Hellman and R. R. Weichselbaum, "Oligometastases," J Clin Oncol **13**, 8-10 (1995).

[24] W. G. Ward, K. Mikaelian, F. Dorey, J. M. Mirra, A. Sassoon, E. C. Holmes, F. R. Eilber and J. J. Eckardt, "Pulmonary metastases of stage IIB extremity osteosarcoma and subsequent pulmonary metastases," J Clin Oncol **12**, 1849-1858 (1994).

[25] "Long-term results of lung metastasectomy: prognostic analyses based on 5206 cases. The International Registry of Lung Metastases," J Thorac Cardiovasc Surg **113**, 37-49 (1997).

[26] A. J. Fakiris, R. C. McGarry, C. T. Yiannoutsos, L. Papiez, M. Williams, M. A. Henderson and R. Timmerman, "Stereotactic body radiation therapy for early-stage non-small-cell lung carcinoma: four-year results of a prospective phase II study," Int J Radiat Oncol Biol Phys **75**, 677-682 (2009).

[27] P. Baumann, J. Nyman, M. Hoyer, B. Wennberg, G. Gagliardi, I. Lax, N. Drugge, L. Ekberg, S. Friesland, K. A. Johansson, J. A. Lund, E. Morhed, K. Nilsson, N. Levin, M. Paludan, C. Sederholm, A. Traberg, L. Wittgren and R. Lewensohn, "Outcome in a Prospective Phase II Trial of Medically Inoperable Stage I Non-Small-Cell Lung Cancer Patients Treated With Stereotactic Body Radiotherapy," J Clin Oncol (2009).

[28] U. Ricardi, A. R. Filippi, A. Guarneri, F. R. Giglioli, P. Ciammella, P. Franco, C. Mantovani, P. Borasio, G. V. Scagliotti and R. Ragona, "Stereotactic body radiation therapy for early stage non-small cell lung cancer: Results of a prospective trial," Lung Cancer (2009).

[29] M. Koto, Y. Takai, Y. Ogawa, H. Matsushita, K. Takeda, C. Takahashi, K. R. Britton, K. Jingu, K. Takai, M. Mitsuya, K. Nemoto and S. Yamada, "A phase II study on stereotactic body radiotherapy for stage I non-small cell lung cancer," Radiother Oncol **85**, 429-434 (2007).

[30] R. C. McGarry, L. Papiez, M. Williams, T. Whitford and R. D. Timmerman, "Stereotactic body radiation therapy of early-stage non-small-cell lung carcinoma: phase I study," Int J Radiat Oncol Biol Phys **63**, 1010-1015 (2005).

[31] S. Hellman and R. R. Weichselbaum, "Importance of local control in an era of systemic therapy," Nat Clin Pract Oncol **2**, 60-61 (2005).

[32] N. Mehta, A. M. Mauer, S. Hellman, D. J. Haraf, E. E. Cohen, E. E. Vokes and R. R. Weichselbaum, "Analysis of further disease progression in metastatic non-small cell lung cancer: implications for locoregional treatment," Int J Oncol **25**, 1677-1683 (2004).

[33] D. M. Macdermed, R. R. Weichselbaum and J. K. Salama, "A rationale for the targeted treatment of oligometastases with radiotherapy," J Surg Oncol **98**, 202-206 (2008).

[34] H. Blomgren, I. Lax, I. Naslund and R. Svanstrom, "Stereotactic high dose fraction radiation therapy of extracranial tumors using an accelerator. Clinical experience of the first thirty-one patients," Acta Oncol **34**, 861-870 (1995).

[35] Y. Nagata, Y. Negoro, T. Aoki, T. Mizowaki, K. Takayama, M. Kokubo, N. Araki, M. Mitsumori, K. Sasai, Y. Shibamoto, S. Koga, S. Yano and M. Hiraoka, "Clinical outcomes of 3D conformal hypofractionated single high-dose radiotherapy for one or two lung tumors using a stereotactic body frame," Int J Radiat Oncol Biol Phys **52**, 1041-1046 (2002).

[36] R. Onimaru, H. Shirato, S. Shimizu, K. Kitamura, B. Xu, S. Fukumoto, T. C. Chang, K. Fujita, M. Oita, K. Miyasaka, M. Nishimura and H. Dosaka-Akita, "Tolerance of organs at risk in small-volume, hypofractionated, image-guided radiotherapy for primary and metastatic lung cancers," Int J Radiat Oncol Biol Phys **56**, 126-135 (2003).

[37] J. Wulf, U. Haedinger, U. Oppitz, W. Thiele, G. Mueller and M. Flentje, "Stereotactic radiotherapy for primary lung cancer and pulmonary metastases: a noninvasive treatment approach in medically inoperable patients," Int J Radiat Oncol Biol Phys **60**, 186-196 (2004).

[38] K. E. Rusthoven, B. D. Kavanagh, S. H. Burri, C. Chen, H. Cardenes, M. A. Chidel, T. J. Pugh, M. Kane, L. E. Gaspar and T. E. Schefter, "Multi-institutional phase I/II trial of stereotactic body radiation therapy for lung metastases," J Clin Oncol **27**, 1579-1584 (2009).

[39] L. B. Marks, E. D. Yorke, A. Jackson, R. K. Ten Haken, L. S. Constine, A. Eisbruch, S. M. Bentzen, J. Nam and J. O. Deasy, "Use of normal tissue complication probability models in the clinic," Int J Radiat Oncol Biol Phys **76**, S10-19 (2010).

[40] S. H. Benedict, K. M. Yenice, D. Followill, J. M. Galvin, W. Hinson, B. Kavanagh, P. Keall, M. Lovelock, S. Meeks, L. Papiez, T. Purdie, R. Sadagopan, M. C. Schell, B. Salter, D. J. Schlesinger, A. S. Shiu, T. Solberg, D. Y. Song, V. Stieber, R. Timmerman, W. A. Tome, D. Verellen, L. Wang and F. F. Yin, "Stereotactic body radiation therapy: the report of AAPM Task Group 101," Med Phys **37**, 4078-4101 (2010).

[41] A. Chi, Z. Liao, N. P. Nguyen, J. Xu, B. Stea and R. Komaki, "Systemic review of the patterns of failure following stereotactic body radiation therapy in early-stage non-small-cell lung cancer: clinical implications," Radiother Oncol **94**, 1-11 (2010).

[42] W. T. Brown, X. Wu, B. Amendola, M. Perman, H. Han, F. Fayad, S. Garcia, A. Lewin, A. Abitbol, A. de la Zerda and J. G. Schwade, "Treatment of early non-small cell lung cancer, stage IA, by image-guided robotic stereotactic radioablation--CyberKnife," Cancer J **13**, 87-94 (2007).

[43] S. Vahdat, E. K. Oermann, S. P. Collins, X. Yu, M. Abedalthagafi, P. Debrito, S. Suy, S. Yousefi, C. J. Gutierrez, T. Chang, F. Banovac, E. D. Anderson, G. Esposito and B. T. Collins, "CyberKnife radiosurgery for inoperable stage IA non-small cell lung cancer: 18F-fluorodeoxyglucose positron emission tomography/computed tomography serial tumor response assessment," J Hematol Oncol **3**, 6 (2010).

[44] A. Chi, S. Y. Jang, J. S. Welsh, N. P. Nguyen, E. Ong, L. Gobar and R. Komaki, "Feasibility of Helical Tomotherapy in Stereotactic Body Radiation Therapy for Centrally Located Early Stage Nonsmall-cell Lung Cancer or Lung Metastases," Int J Radiat Oncol Biol Phys (2011).

[45] J. Zhou, B. Uhl, K. Dewitt, M. Young, B. Taylor, D. Y. Fei and Y. C. Lo, "Image-guided stereotactic body radiotherapy for lung tumors using BodyLoc with tomotherapy: clinical implementation and set-up accuracy," Med Dosim **35**, 12-18 (2010).

[46] J. M. Baisden, D. A. Romney, A. G. Reish, J. Cai, K. Sheng, D. R. Jones, S. H. Benedict, P. W. Read and J. M. Larner, "Dose as a function of lung volume and planned treatment volume in helical tomotherapy intensity-modulated radiation therapy-based stereotactic body radiation therapy for small lung tumors," Int J Radiat Oncol Biol Phys **68**, 1229-1237 (2007).

[47] C. Ding, C. H. Chang, J. Haslam, R. Timmerman and T. Solberg, "A dosimetric comparison of stereotactic body radiation therapy techniques for lung cancer: robotic versus conventional linac-based systems," J Appl Clin Med Phys **11**, 3223 (2010).

[48] P. Mavroidis, B. C. Ferreira, C. Shi, B. K. Lind and N. Papanikolaou, "Treatment plan comparison between helical tomotherapy and MLC-based IMRT using radiobiological measures," Phys Med Biol **52**, 3817-3836 (2007).

[49] G. M. Videtic, K. Stephans, C. Reddy, S. Gajdos, M. Kolar, E. Clouser and T. Djemil, "Intensity-modulated radiotherapy-based stereotactic body radiotherapy for medically inoperable

early-stage lung cancer: excellent local control," Int J Radiat Oncol Biol Phys **77**, 344-349 (2010).

[50] A. Holt, C. van Vliet-Vroegindeweij, A. Mans, J. S. Belderbos and E. M. Damen, "Volumetric-Modulated Arc Therapy for Stereotactic Body Radiotherapy of Lung Tumors: A Comparison With Intensity-Modulated Radiotherapy Techniques," Int J Radiat Oncol Biol Phys (2011).

[51] J. Brock, J. Bedford, M. Partridge, F. McDonald, S. Ashley, H. A. McNair and M. Brada, "Optimising Stereotactic Body Radiotherapy for Non-small Cell Lung Cancer with Volumetric Intensity-modulated Arc Therapy-A Planning Study," Clin Oncol (R Coll Radiol) (2011).

[52] D. A. Palma, S. Senan, C. J. Haasbeek, W. F. Verbakel, A. Vincent and F. Lagerwaard, "Radiological and clinical pneumonitis after stereotactic lung radiotherapy: a matched analysis of three-dimensional conformal and volumetric-modulated arc therapy techniques," Int J Radiat Oncol Biol Phys **80**, 506-513 (2011).

[53] J. T. Leith, S. Cook, P. Chougule, P. Calabresi, L. Wahlberg, C. Lindquist and M. Epstein, "Intrinsic and extrinsic characteristics of human tumors relevant to radiosurgery: comparative cellular radiosensitivity and hypoxic percentages," Acta Neurochir Suppl **62**, 18-27 (1994).

[54] J. M. Galvin, G. Ezzell, A. Eisbrauch, C. Yu, B. Butler, Y. Xiao, I. Rosen, J. Rosenman, M. Sharpe, L. Xing, P. Xia, T. Lomax, D. A. Low and J. Palta, "Implementing IMRT in clinical practice: a joint document of the American Society for Therapeutic Radiology and Oncology and the American Association of Physicists in Medicine," Int J Radiat Oncol Biol Phys **58**, 1616-1634 (2004).

[55] R. Mohan, M. Arnfield, S. Tong, Q. Wu and J. Siebers, "The impact of fluctuations in intensity patterns on the number of monitor units and the quality and accuracy of intensity modulated radiotherapy," Med Phys **27**, 1226-1237 (2000).

[56] S. F. Kry, M. Salehpour, D. S. Followill, M. Stovall, D. A. Kuban, R. A. White and Rosen, II, "The calculated risk of fatal secondary malignancies from intensity-modulated radiation therapy," Int J Radiat Oncol Biol Phys **62**, 1195-1203 (2005).

[57] T. Bortfeld, K. Jokivarsi, M. Goitein, J. Kung and S. B. Jiang, "Effects of intra-fraction motion on IMRT dose delivery: statistical analysis and simulation," Phys Med Biol **47**, 2203-2220 (2002).

[58] S. B. Jiang, C. Pope, K. M. Al Jarrah, J. H. Kung, T. Bortfeld and G. T. Chen, "An experimental investigation on intra-fractional organ motion effects in lung IMRT treatments," Phys Med Biol **48**, 1773-1784 (2003).

[59] C. S. Chui, E. Yorke and L. Hong, "The effects of intra-fraction organ motion on the delivery of intensity-modulated field with a multileaf collimator," Med Phys **30**, 1736-1746 (2003).

[60] M. Schaefer, M. W. Munter, C. Thilmann, F. Sterzing, P. Haering, S. E. Combs and J. Debus, "Influence of intra-fractional breathing movement in step-and-shoot IMRT," Phys Med Biol **49**, N175-179 (2004).

[61] S. Kamath, S. Sahni, J. Palta and S. Ranka, "Algorithms for optimal sequencing of dynamic multileaf collimators," Phys Med Biol **49**, 33-54 (2004).

[62] D. Georg, B. Kroupa, P. Georg, P. Winkler, J. Bogner, K. Dieckmann and R. Potter, "Inverse planning--a comparative intersystem and interpatient constraint study," Strahlenther Onkol **182**, 473-480 (2006).

[63] D. M. Shepard, M. A. Earl, X. A. Li, S. Naqvi and C. Yu, "Direct aperture optimization: a turnkey solution for step-and-shoot IMRT," Med Phys **29**, 1007-1018 (2002).

[64] P. Dvorak, D. Georg, J. Bogner, B. Kroupa, K. Dieckmann and R. Potter, "Impact of IMRT and leaf width on stereotactic body radiotherapy of liver and lung lesions," Int J Radiat Oncol Biol Phys **61**, 1572-1581 (2005).

65 T. Krieger and O. A. Sauer, "Monte Carlo- versus pencil-beam-/collapsed-cone-dose calculation in a heterogeneous multi-layer phantom," Phys Med Biol **50**, 859-868 (2005).

66 T. Knoos, E. Wieslander, L. Cozzi, C. Brink, A. Fogliata, D. Albers, H. Nystrom and S. Lassen, "Comparison of dose calculation algorithms for treatment planning in external photon beam therapy for clinical situations," Phys Med Biol **51**, 5785-5807 (2006).

67 D. Craft, T. Halabi, H. A. Shih and T. Bortfeld, "An approach for practical multiobjective IMRT treatment planning," Int J Radiat Oncol Biol Phys **69**, 1600-1607 (2007).

68 Z. Jiang, M. A. Earl, G. W. Zhang, C. X. Yu and D. M. Shepard, "An examination of the number of required apertures for step-and-shoot IMRT," Phys Med Biol **50**, 5653-5663 (2005).

69 M. Pepin, P. Dufour, M. Lambert, M. Aubert, A. Valognes, T. Rotis, A. Van de Wiele and D. Bergonier, "Comparison of three enzyme-linked immunosorbent assays for serologic diagnosis of contagious agalactia in sheep," J Vet Diagn Invest **15**, 281-285 (2003).

70 C. W. Stevens, R. F. Munden, K. M. Forster, J. F. Kelly, Z. Liao, G. Starkschall, S. Tucker and R. Komaki, "Respiratory-driven lung tumor motion is independent of tumor size, tumor location, and pulmonary function," Int J Radiat Oncol Biol Phys **51**, 62-68 (2001).

71 J. R. van Sornsen de Koste, F. J. Lagerwaard, M. R. Nijssen-Visser, W. J. Graveland and S. Senan, "Tumor location cannot predict the mobility of lung tumors: a 3D analysis of data generated from multiple CT scans," Int J Radiat Oncol Biol Phys **56**, 348-354 (2003).

72 T. Aruga, J. Itami, M. Aruga, K. Nakajima, K. Shibata, T. Nojo, S. Yasuda, T. Uno, R. Hara, K. Isobe, N. Machida and H. Ito, "Target volume definition for upper abdominal irradiation using CT scans obtained during inhale and exhale phases," Int J Radiat Oncol Biol Phys **48**, 465-469 (2000).

73 F. J. Lagerwaard, J. R. Van Sornsen de Koste, M. R. Nijssen-Visser, R. H. Schuchhard-Schipper, S. S. Oei, A. Munne and S. Senan, "Multiple "slow" CT scans for incorporating lung tumor mobility in radiotherapy planning," Int J Radiat Oncol Biol Phys **51**, 932-937 (2001).

74 B. J. Slotman, F. J. Lagerwaard and S. Senan, "4D imaging for target definition in stereotactic radiotherapy for lung cancer," Acta Oncol **45**, 966-972 (2006).

75 T. G. Purdie, D. J. Moseley, J. P. Bissonnette, M. B. Sharpe, K. Franks, A. Bezjak and D. A. Jaffray, "Respiration correlated cone-beam computed tomography and 4DCT for evaluating target motion in Stereotactic Lung Radiation Therapy," Acta Oncol **45**, 915-922 (2006).

76 R. W. Underberg, F. J. Lagerwaard, B. J. Slotman, J. P. Cuijpers and S. Senan, "Benefit of respiration-gated stereotactic radiotherapy for stage I lung cancer: an analysis of 4DCT datasets," Int J Radiat Oncol Biol Phys **62**, 554-560 (2005).

77 J. D. Bradley, A. N. Nofal, I. M. El Naqa, W. Lu, J. Liu, J. Hubenschmidt, D. A. Low, R. E. Drzymala and D. Khullar, "Comparison of helical, maximum intensity projection (MIP), and averaged intensity (AI) 4D CT imaging for stereotactic body radiation therapy (SBRT) planning in lung cancer," Radiother Oncol **81**, 264-268 (2006).

78 M. Nakamura, Y. Narita, Y. Matsuo, M. Narabayashi, M. Nakata, S. Yano, Y. Miyabe, K. Matsugi, A. Sawada, Y. Norihisa, T. Mizowaki, Y. Nagata and M. Hiraoka, "Geometrical differences in target volumes between slow CT and 4D CT imaging in stereotactic body radiotherapy for lung tumors in the upper and middle lobe," Med Phys **35**, 4142-4148 (2008).

79 P. Fritz, H. J. Kraus, T. Blaschke, W. Muhlnickel, K. Strauch, W. Engel-Riedel, A. Chemaissani and E. Stoelben, "Stereotactic, high single-dose irradiation of stage I non-small cell lung cancer (NSCLC) using four-dimensional CT scans for treatment planning," Lung Cancer **60**, 193-199 (2008).

80 J. Hanley, M. M. Debois, D. Mah, G. S. Mageras, A. Raben, K. Rosenzweig, B. Mychalczak, L. H. Schwartz, P. J. Gloeggler, W. Lutz, C. C. Ling, S. A. Leibel, Z. Fuks and G. J. Kutcher, "Deep inspiration breath-hold technique for lung tumors: the potential value of target immobilization and reduced lung density in dose escalation," Int J Radiat Oncol Biol Phys **45**, 603-611 (1999).

81 J. W. Wong, M. B. Sharpe, D. A. Jaffray, V. R. Kini, J. M. Robertson, J. S. Stromberg and A. A. Martinez, "The use of active breathing control (ABC) to reduce margin for breathing motion," Int J Radiat Oncol Biol Phys **44**, 911-919 (1999).

[82] D. J. Kim, B. R. Murray, R. Halperin and W. H. Roa, "Held-breath self-gating technique for radiotherapy of non-small-cell lung cancer: a feasibility study," Int J Radiat Oncol Biol Phys **49**, 43-49 (2001).

[83] I. Lax, H. Blomgren, I. Naslund and R. Svanstrom, "Stereotactic radiotherapy of malignancies in the abdomen. Methodological aspects," Acta Oncol **33**, 677-683 (1994).

[84] Y. Negoro, Y. Nagata, T. Aoki, T. Mizowaki, N. Araki, K. Takayama, M. Kokubo, S. Yano, S. Koga, K. Sasai, Y. Shibamoto and M. Hiraoka, "The effectiveness of an immobilization device in conformal radiotherapy for lung tumor: reduction of respiratory tumor movement and evaluation of the daily setup accuracy," Int J Radiat Oncol Biol Phys **50**, 889-898 (2001).

[85] H. D. Kubo and B. C. Hill, "Respiration gated radiotherapy treatment: a technical study," Phys Med Biol **41**, 83-91 (1996).

[86] A. M. Berson, R. Emery, L. Rodriguez, G. M. Richards, T. Ng, S. Sanghavi and J. Barsa, "Clinical experience using respiratory gated radiation therapy: comparison of free-breathing and breath-hold techniques," Int J Radiat Oncol Biol Phys **60**, 419-426 (2004).

[87] G. S. Mageras and E. Yorke, "Deep inspiration breath hold and respiratory gating strategies for reducing organ motion in radiation treatment," Semin Radiat Oncol **14**, 65-75 (2004).

[88] P. J. Keall, G. S. Mageras, J. M. Balter, R. S. Emery, K. M. Forster, S. B. Jiang, J. M. Kapatoes, D. A. Low, M. J. Murphy, B. R. Murray, C. R. Ramsey, M. B. Van Herk, S. S. Vedam, J. W. Wong and E. Yorke, "The management of respiratory motion in radiation oncology report of AAPM Task Group 76," Med Phys **33**, 3874-3900 (2006).

[89] H. Shirato, S. Shimizu, T. Kunieda, K. Kitamura, M. van Herk, K. Kagei, T. Nishioka, S. Hashimoto, K. Fujita, H. Aoyama, K. Tsuchiya, K. Kudo and K. Miyasaka, "Physical aspects of a real-time tumor-tracking system for gated radiotherapy," Int J Radiat Oncol Biol Phys **48**, 1187-1195 (2000).

[90] L. C. Fang, R. Komaki, P. Allen, T. Guerrero, R. Mohan and J. D. Cox, "Comparison of outcomes for patients with medically inoperable Stage I non-small-cell lung cancer treated with two-dimensional vs. three-dimensional radiotherapy," Int J Radiat Oncol Biol Phys **66**, 108-116 (2006).

[91] Y. Seppenwoolde, H. Shirato, K. Kitamura, S. Shimizu, M. van Herk, J. V. Lebesque and K. Miyasaka, "Precise and real-time measurement of 3D tumor motion in lung due to breathing and heartbeat, measured during radiotherapy," Int J Radiat Oncol Biol Phys **53**, 822-834 (2002).

[92] J. Wulf, U. Hadinger, U. Oppitz, B. Olshausen and M. Flentje, "Stereotactic radiotherapy of extracranial targets: CT-simulation and accuracy of treatment in the stereotactic body frame," Radiother Oncol **57**, 225-236 (2000).

[93] F. Lohr, J. Debus, C. Frank, K. Herfarth, O. Pastyr, B. Rhein, M. L. Bahner, W. Schlegel and M. Wannenmacher, "Noninvasive patient fixation for extracranial stereotactic radiotherapy," Int J Radiat Oncol Biol Phys **45**, 521-527 (1999).

[94] Z. Wang, J. W. Nelson, S. Yoo, Q. J. Wu, J. P. Kirkpatrick, L. B. Marks and F. F. Yin, "Refinement of treatment setup and target localization accuracy using three-dimensional cone-

beam computed tomography for stereotactic body radiotherapy," Int J Radiat Oncol Biol Phys **73**, 571-577 (2009).

[95] J. J. Sonke, M. Rossi, J. Wolthaus, M. van Herk, E. Damen and J. Belderbos, "Frameless stereotactic body radiotherapy for lung cancer using four-dimensional cone beam CT guidance," Int J Radiat Oncol Biol Phys **74**, 567-574 (2009).

[96] Cancer Therapy Evaluation Program. Available at http://evs.nci.nih.gov/

[97] R. Mohan, G. S. Mageras, B. Baldwin, L. J. Brewster, G. J. Kutcher, S. Leibel, C. M. Burman, C. C. Ling and Z. Fuks, "Clinically relevant optimization of 3-D conformal treatments," Med Phys **19**, 933-944 (1992).

[98] J. T. Lyman, "Complication probability as assessed from dose-volume histograms," Radiat Res Suppl **8**, S13-19 (1985).

[99] G. J. Kutcher and C. Burman, "Calculation of complication probability factors for non-uniform normal tissue irradiation: the effective volume method," Int J Radiat Oncol Biol Phys **16**, 1623-1630 (1989).

[100] M. V. Graham, J. A. Purdy, B. Emami, W. Harms, W. Bosch, M. A. Lockett and C. A. Perez, "Clinical dose-volume histogram analysis for pneumonitis after 3D treatment for non-small cell lung cancer (NSCLC)," Int J Radiat Oncol Biol Phys **45**, 323-329 (1999).

[101] E. D. Yorke, A. Jackson, K. E. Rosenzweig, L. Braban, S. A. Leibel and C. C. Ling, "Correlation of dosimetric factors and radiation pneumonitis for non-small-cell lung cancer patients in a recently completed dose escalation study," Int J Radiat Oncol Biol Phys **63**, 672-682 (2005).

[102] T. Uno, K. Isobe, H. Kawakami, N. Ueno, T. Kawata, S. Yamamoto, Y. Sekine, A. Iyoda, T. Iizasa, T. Fujisawa, N. Shigematsu and H. Ito, "Dose-volume factors predicting radiation

pneumonitis in patients receiving salvage radiotherapy for postlobectomy locoregional recurrent non-small-cell lung cancer," Int J Clin Oncol **11**, 55-59 (2006).

[103] F. M. Kong, J. A. Hayman, K. A. Griffith, G. P. Kalemkerian, D. Arenberg, S. Lyons, A. Turrisi, A. Lichter, B. Fraass, A. Eisbruch, T. S. Lawrence and R. K. Ten Haken, "Final toxicity results of a radiation-dose escalation study in patients with non-small-cell lung cancer (NSCLC): predictors for radiation pneumonitis and fibrosis," Int J Radiat Oncol Biol Phys **65**, 1075-1086 (2006).

[104] I. Kyas, H. Hof, J. Debus, W. Schlegel and C. P. Karger, "Prediction of radiation-induced changes in the lung after stereotactic body radiation therapy of non-small-cell lung cancer," Int J Radiat Oncol Biol Phys **67**, 768-774 (2007).

[105] V. A. Semenenko, R. C. Molthen, C. Li, N. V. Morrow, R. Li, S. N. Ghosh, M. M. Medhora and X. A. Li, "Irradiation of varying volumes of rat lung to same mean lung dose: a little to a lot or a lot to a little?," Int J Radiat Oncol Biol Phys **71**, 838-847 (2008).

[106] G. R. Borst, M. Ishikawa, J. Nijkamp, M. Hauptmann, H. Shirato, R. Onimaru, M. M. van den Heuvel, J. Belderbos, J. V. Lebesque and J. J. Sonke, "Radiation pneumonitis in patients treated for malignant pulmonary lesions with hypofractionated radiation therapy," Radiother Oncol **91**, 307-313 (2009).

[107] M. Guckenberger, K. Baier, B. Polat, A. Richter, T. Krieger, J. Wilbert, G. Mueller and M. Flentje, "Dose-response relationship for radiation-induced pneumonitis after pulmonary stereotactic body radiotherapy," Radiother Oncol **97**, 65-70 (2010).

[108] D. J. Brenner, "The linear-quadratic model is an appropriate methodology for determining isoeffective doses at large doses per fraction," Semin Radiat Oncol **18**, 234-239 (2008).

[109] J. P. Kirkpatrick, J. J. Meyer and L. B. Marks, "The linear-quadratic model is inappropriate to model high dose per fraction effects in radiosurgery," Semin Radiat Oncol **18**, 240-243 (2008).

[110] M. Guckenberger, J. Wulf, G. Mueller, T. Krieger, K. Baier, M. Gabor, A. Richter, J. Wilbert and M. Flentje, "Dose-response relationship for image-guided stereotactic body radiotherapy of pulmonary tumors: relevance of 4D dose calculation," Int J Radiat Oncol Biol Phys **74**, 47-54 (2009).

[111] H. Onishi, H. Shirato, Y. Nagata, M. Hiraoka, M. Fujino, K. Gomi, Y. Niibe, K. Karasawa, K. Hayakawa, Y. Takai, T. Kimura, A. Takeda, A. Ouchi, M. Hareyama, M. Kokubo, R. Hara, J. Itami, K. Yamada and T. Araki, "Hypofractionated stereotactic radiotherapy (HypoFXSRT) for stage I non-small cell lung cancer: updated results of 257 patients in a Japanese multi-institutional study," J Thorac Oncol **2**, S94-100 (2007).

[112] R. Onimaru, M. Fujino, K. Yamazaki, Y. Onodera, H. Taguchi, N. Katoh, F. Hommura, S. Oizumi, M. Nishimura and H. Shirato, "Steep dose-response relationship for stage I non-small-cell lung cancer using hypofractionated high-dose irradiation by real-time tumor-tracking radiotherapy," Int J Radiat Oncol Biol Phys **70**, 374-381 (2008).

[113] T. T. Puck and P. I. Marcus, "Action of x-rays on mammalian cells," J Exp Med **103**, 653-666 (1956).

[114] M. Guerrero and X. A. Li, "Extending the linear-quadratic model for large fraction doses pertinent to stereotactic radiotherapy," Phys Med Biol **49**, 4825-4835 (2004).

[115] G. R. Borst, M. Ishikawa, J. Nijkamp, M. Hauptmann, H. Shirato, G. Bengua, R. Onimaru, A. de Josien Bois, J. V. Lebesque and J. J. Sonke, "Radiation pneumonitis after hypofractionated radiotherapy: evaluation of the LQ(L) model and different dose parameters," Int J Radiat Oncol Biol Phys **77**, 1596-1603 (2010).

[116] R. Timmerman, R. McGarry, C. Yiannoutsos, L. Papiez, K. Tudor, J. DeLuca, M. Ewing, R. Abdulrahman, C. DesRosiers, M. Williams and J. Fletcher, "Excessive toxicity when treating

central tumors in a phase II study of stereotactic body radiation therapy for medically inoperable early-stage lung cancer," J Clin Oncol **24**, 4833-4839 (2006).

[117] M. A. Chaudhry, "Bystander effect: biological endpoints and microarray analysis," Mutat Res **597**, 98-112 (2006).

[118] M. A. Khan, R. P. Hill and J. Van Dyk, "Partial volume rat lung irradiation: an evaluation of early DNA damage," Int J Radiat Oncol Biol Phys **40**, 467-476 (1998).

[119] K. R. Arbetter, U. B. Prakash, H. D. Tazelaar and W. W. Douglas, "Radiation-induced pneumonitis in the "nonirradiated" lung," Mayo Clin Proc **74**, 27-36 (1999).

[120] C. Martin, S. Romero, J. Sanchez-Paya, B. Massuti, J. M. Arriero and L. Hernandez, "Bilateral lymphocytic alveolitis: a common reaction after unilateral thoracic irradiation," Eur Respir J **13**, 727-732 (1999).

[121] G. W. Morgan and S. N. Breit, "Radiation and the lung: a reevaluation of the mechanisms mediating pulmonary injury," Int J Radiat Oncol Biol Phys **31**, 361-369 (1995).

[122] L. Feuvret, G. Noel, J. J. Mazeron and P. Bey, "Conformity index: a review," Int J Radiat Oncol Biol Phys **64**, 333-342 (2006).

[123] T. Knoos, I. Kristensen and P. Nilsson, "Volumetric and dosimetric evaluation of radiation treatment plans: radiation conformity index," Int J Radiat Oncol Biol Phys **42**, 1169-1176 (1998).

[124] R. Timmerman, J. Galvin, J. Michalski, W. Straube, G. Ibbott, E. Martin, R. Abdulrahman, S. Swann, J. Fowler and H. Choy, "Accreditation and quality assurance for Radiation Therapy Oncology Group: Multicenter clinical trials using Stereotactic Body Radiation Therapy in lung cancer," Acta Oncol **45**, 779-786 (2006).

[125] H. Yamashita, K. Nakagawa, N. Nakamura, H. Koyanagi, M. Tago, H. Igaki, K. Shiraishi, N. Sasano and K. Ohtomo, "Exceptionally high incidence of symptomatic Grade 2-5 radiation pneumonitis after stereotactic radiation therapy for lung tumors," Radiat Oncol **2**, 21 (2007).

[126] E. J. Hall and C. S. Wuu, "Radiation-induced second cancers: the impact of 3D-CRT and IMRT," Int J Radiat Oncol Biol Phys **56**, 83-88 (2003).

[127] E. K. Rofstad, K. Sundfor, H. Lyng and C. G. Trope, "Hypoxia-induced treatment failure in advanced squamous cell carcinoma of the uterine cervix is primarily due to hypoxia-induced radiation resistance rather than hypoxia-induced metastasis," Br J Cancer **83**, 354-359 (2000).

[128] J. M. Brown, "Exploiting the hypoxic cancer cell: mechanisms and therapeutic strategies," Mol Med Today **6**, 157-162 (2000).

[129] D. Coon, A. S. Gokhale, S. A. Burton, D. E. Heron, C. Ozhasoglu and N. Christie, "Fractionated stereotactic body radiation therapy in the treatment of primary, recurrent, and metastatic lung tumors: the role of positron emission tomography/computed tomography-based treatment planning," Clin Lung Cancer **9**, 217-221 (2008).

[130] R. E. Wurm, F. Gum, S. Erbel, L. Schlenger, D. Scheffler, D. Agaoglu, R. Schild, B. Gebauer, P. Rogalla, M. Plotkin, K. Ocran and V. Budach, "Image guided respiratory gated hypofractionated Stereotactic Body Radiation Therapy (H-SBRT) for liver and lung tumors: Initial experience," Acta Oncol **45**, 881-889 (2006).

[131] D. A. Low, "Quality assurance of intensity-modulated radiotherapy," Semin Radiat Oncol **12**, 219-228 (2002).

[132] D. A. Low, J. M. Moran, J. F. Dempsey, L. Dong and M. Oldham, "Dosimetry tools and techniques for IMRT," Med Phys **38**, 1313-1338 (2011).

[133] Y. Zhu, A. S. Kirov, V. Mishra, A. S. Meigooni and J. F. Williamson, "Quantitative evaluation of radiochromic film response for two-dimensional dosimetry," Med Phys **24**, 223-231 (1997).

[134] D. A. Low, W. B. Harms, S. Mutic and J. A. Purdy, "A technique for the quantitative evaluation of dose distributions," Med Phys **25**, 656-661 (1998).

[135] M. Essers and B. J. Mijnheer, "In vivo dosimetry during external photon beam radiotherapy," Int J Radiat Oncol Biol Phys **43**, 245-259 (1999).

[136] A. Ismail, J. Y. Giraud, G. N. Lu, R. Sihanath, P. Pittet, J. M. Galvan and J. Balosso, "Radiotherapy quality assurance by individualized in vivo dosimetry: state of the art," Cancer Radiother **13**, 182-189 (2009).

[137] T. E. Burlin, "A general theory of cavity ionisation," Br J Radiol **39**, 727-734 (1966).

[138] R. I. Berbeco, C. J. Pope and S. B. Jiang, "Measurement of the interplay effect in lung IMRT treatment using EDR2 films," J Appl Clin Med Phys **7**, 33-42 (2006).

[139] S. Sura, V. Gupta, E. Yorke, A. Jackson, H. Amols and K. E. Rosenzweig, "Intensity-modulated radiation therapy (IMRT) for inoperable non-small cell lung cancer: the Memorial Sloan-Kettering Cancer Center (MSKCC) experience," Radiother Oncol **87**, 17-23 (2008).

[140] Z. Q. Jiang, K. Yang, R. Komaki, X. Wei, S. L. Tucker, Y. Zhuang, M. K. Martel, S. Vedam, P. Balter, G. Zhu, D. Gomez, C. Lu, R. Mohan, J. D. Cox and Z. Liao, "Long-Term Clinical Outcome of Intensity-Modulated Radiotherapy for Inoperable Non-Small-Cell Lung Cancer: The MD Anderson Experience," Int J Radiat Oncol Biol Phys (2011).

[141] H. Kang, E. D. Yorke, J. Yang, C. S. Chui, K. E. Rosenzweig and H. I. Amols, "Evaluation of tumor motion effects on dose distribution for hypofractionated intensity-modulated radiotherapy of non-small-cell lung cancer," J Appl Clin Med Phys **11**, 3182 (2010).

[142] J. Seco, G. C. Sharp, J. Turcotte, D. Gierga, T. Bortfeld and H. Paganetti, "Effects of organ motion on IMRT treatments with segments of few monitor units," Med Phys **34**, 923-934 (2007).

[143] E. E. Klein, A. Morrison, J. A. Purdy, M. V. Graham and J. Matthews, "A volumetric study of measurements and calculations of lung density corrections for 6 and 18 MV photons," Int J Radiat Oncol Biol Phys **37**, 1163-1170 (1997).

[144] M. E. Young and R. O. Kornelsen, "Dose corrections for low-density tissue inhomogeneities and air channels for 10-MV x rays," Med Phys **10**, 450-455 (1983).

[145] P. J. White, R. D. Zwicker and D. T. Huang, "Comparison of dose homogeneity effects due to electron equilibrium loss in lung for 6 MV and 18 MV photons," Int J Radiat Oncol Biol Phys **34**, 1141-1146 (1996).

[146] K. Mah and J. Van Dyk, "On the impact of tissue inhomogeneity corrections in clinical thoracic radiation therapy," Int J Radiat Oncol Biol Phys **21**, 1257-1267 (1991).

VITA

Name:	Julien Avi Dan Partouche Sebban
Address:	Nuclear Engineering Department 337 Zachry Engineering Building, 3133 TAMU College Station, TX 77843-3133
Email Address:	julien@tamu.edu
Education:	M.E., Electronic and Telecommunication, Fondation EPF Sceaux, France, 2002 M.S., Health Physics, Texas A&M University, 2006 PhD., Nuclear Engineering, Texas A&M University, 2012